

# Induced Gravitational Waves from Multi-Sound Speed Resonances during Cosmological Inflation

Andrea Addazi\*

*Center for Theoretical Physics, College of Physics,  
Sichuan University, Chengdu, 610064, PR China and  
Laboratori Nazionali di Frascati INFN, Frascati (Rome), Italy, EU*

Salvatore Capozziello<sup>†</sup>

*Dipartimento di Fisica E. Pancini, Università di Napoli Federico II and Istituto Nazionale di Fisica Nucleare,  
Sezione di Napoli, Compl. Univ. di Monte S. Angelo,  
Edificio G, Via Cinthia, I-80126, Napoli, Italy, and  
Scuola Superiore Meridionale, Largo S. Marcellino 10, I-80138, Napoli, Italy,*

Qingyu Gan<sup>‡</sup>

*Center for Theoretical Physics, College of Physics,  
Sichuan University, Chengdu, 610064, PR China and  
Scuola Superiore Meridionale, Largo S. Marcellino 10, I-80138, Napoli, Italy,*

We explore the possibility of multi-parametric resonances from time varying sound speed during cosmological inflation. In particular, we fix our set-up to the simpler case beyond a single oscillation model already explored in literature: two sinusoidal harmonics around a constant sound speed equal to one. We find that, within the perturbative regime, except for some certain extreme corners of the parameter space, the primordial density spectrum is characterized by two groups of amplified peaks centered around two critical oscillatory frequencies of the sound speed. As a general result, we show that the energy spectrum of the secondary induced GWs from the inflationary era has a single major broad peak, whereas the one from the radiation dominated phase consists of one/two principle peak-like configuration(s) for relatively small/large ratio of two oscillatory frequencies. The GW relic stochastic backgrounds carry a gravitational memory of the parametric resonances during inflation. GW signals from double sound speed resonances can be tested in complementary channels from Pulsar-timing radio-astronomy, space and terrestrial GW interferometers.

PACS numbers: 04.50.Kd, 04.30.-w, 98.80.-k

arXiv:2204.07668v3 [astro-ph.CO] 6 Aug 2022

---

\* [Addazi@scu.edu.cn](mailto:Addazi@scu.edu.cn)

† [capozziello@unina.it](mailto:capozziello@unina.it)

‡ [gqy@stu.scu.edu.cn](mailto:gqy@stu.scu.edu.cn)

## CONTENTS

I. Introduction	2
II. Sound Speed Resonance and Power Spectrum	3
III. Induced Gravitational Waves in Early Universe	5
A. Radiation Dominated Era	5
B. Inflationary Era	10
IV. Phenomenological Implications	12
V. Discussion and Conclusions	16
References	17

## I. INTRODUCTION

The detection of gravitational waves (GWs) from mergers of binary compact objects [1, 2] also inspire the possibility of searches for stochastic GW backgrounds produced from new physics mechanisms in the early Universe. Indeed, GW physics represents a new arena for tests of fundamental theories in cosmology alongside with the cosmic microwave background (CMB) and large-scale structure (LSS). Cosmological stochastic GW backgrounds can be generated by several different sources. Among all the possibilities, the secondary GW spectrum induced by primordial density perturbations in early universe is particularly interesting and has drawn a lot of attention recently (see for example Ref.[3] for a review in the subject). In the cosmological perturbation theory, it is well known that the scalar and tensor perturbations evolve independently at the linear order while they are dynamically coupled at the second and higher orders [4, 5]. Hence the scalar mode associated with the primordial density perturbations can excite the tensor mode and induce the secondary GWs, when they are either localized at scales much smaller than the Hubble horizon during the inflationary epoch [6–11] or reenter the horizon during the post-inflationary radiation dominated (RD) and matter dominated (MD) eras [12–15]. Such a phenomenon can generate a relic detectable stochastic GW background. CMB and LSS observations imply that primordial fluctuations are distributed as approximately a Gaussian profile at  $\gtrsim 1\text{Mpc}$  scale, with a near scale-invariant power spectrum and an amplitude that is too small to be visible in current detector. Nevertheless, constraints at small scales,  $\ll 1\text{Mpc}$ , are less stringent and a large enhancement of the scalar and tensor fluctuations can be envisaged. Several possible mechanisms for an amplification of primordial density perturbations and induced GWs at small scale were proposed in literature considering local features of the inflaton potential like near-inflection points [16–20], step-like changes [21–23], very small periodic structure [9, 24] and multi-field inflation with a rapid turn [8, 25, 26], higher dimensional operators or non-minimal coupling between inflaton and graviton [27–35], extra axion-like curvaton or spectator scalar field [6, 10, 36–40], first order phase transition [41–43], and supergravity or string inspired models [44–49].

On the other hand, the sound speed of primordial perturbations plays an important role in determining the evolution of Universe in early epoch. Usually, in the standard slow-roll inflation paradigm, the sound speed of the inflaton is equal to one; but it can deviate from the unity in alternative scenarios with non-canonical kinetic term, e.g., k-inflation [50, 51], Dirac-Born-Infeld inflation [52, 53], effective field theory from integrating out the heavy modes [54, 55] and so on. It was extensively explored in the literature that the sizable secondary GWs at small scale can be generated by various behaviors of the varying sound speed of the scalar mode [54–69]. Recently, it was proposed that parametric resonances of primordial density perturbations, originated from the sound speed, with an oscillatory feature in of (conformal) time, can generate a large amplification of the abundance of induced GWs and primordial black holes (PBHs) in the early universe [7, 70–72]. Alternatively, we mention that the parametric resonance can also be achieved considering an oscillatory sound speed of the tensor perturbations during inflation [73].

In this work, we will analyze the primordial GW stochastic background and PBH production in case of multi-sound speed resonances. We will show that the GW relic signals carry a *resonance gravitational memory* of sound speed time-variation during inflation that can be tested in next generation of GW experiments. Multi-parametric resonances may be envisaged in many possible non-minimal coupling and multi-field inflationary dynamics in the early Universe; thus an effective theory approach is of large interest. Indeed, in [70], the modification of the inflaton sound speed by a single cosine function, with the characteristic frequency  $p_*$ , yields resonant modes with wave-number  $k$  around  $p_*$

and a single narrow amplified peak at  $\sim p_*$  in the power spectrum of the primordial curvature perturbation. In a more realistic scenario, it seems natural to generalize such a simple case to sound speed composed of many harmonics as a Fourier series analysis. First, in the single oscillation case, the induced GW spectrum exhibit a single principle peak-like structure and meanwhile PBHs are produced in a narrow mass spectrum. Indeed, secondary resonance peaks in the source spectrum are usually sub-dominated than the major peak by at least  $\sim 5 \div 6$  orders of magnitude [7]. Thus, one efficient way to overcome to it is to consider a modified sound speed with  $n$ -harmonic modes with different frequencies. In this case, one can obtain several resonance peaks corresponding to the  $n$  frequency poles in the power spectrum. Accordingly, we expect to generate the primordial density spectrum with multiple resonating peaks, enhancing the induced GWs with rich multi-peaked features and the formation of PBHs at different mass ranges. Secondly, in [25, 74] the authors showed that the primordial power spectrum can be largely enhanced in a broad regime by a sudden turn of the trajectory in multi-field inflation. Such a change of direction through a different slow-roll hill can cause a complicate oscillation behavior of the sound speed [61, 75], and it can be Fourier decomposed in a complete basis, where each harmonic mode might be responsible for a particular narrow resonance.

As a first step, we focus on the double cosine parameterization, with different amplitudes  $\xi_{*1,2}$  and frequencies  $p_{*1,2}$ . In other words, here we will consider two dominant harmonics in the Fourier expansion, corresponding to the cases where others can be neglected. We will analyze the corresponding resonating pattern of the primordial curvature perturbation and the features of the secondary GWs induced during the inflationary and radiation dominated (RD) eras. We find that, within the perturbative parameter space, there are two groups of amplified peaks around  $p_{*1}$  and  $p_{*2}$  in the scalar power spectrum, which correspond to inflationary induced GWs with a single major broad peak and RD induced GWs with one/two principle peak-like structures for relatively small/large ratio of  $p_{*2}/p_{*1}$  (except some extreme parameter choices that will be discussed later on in details). Let us mention that the double peak structure of the primordial density power spectrum were also explored in Refs.[76–81]. Additionally, on top of the main features of the induced GW spectrum, we will show that there are certain fine structures produced by interactions of the multiple peaks of the source spectrum or the oscillatory modulation of the envelope of particular resonating modes. Furthermore, the single and double cosine oscillatory pattern of the sound speed provide us many hints for more general  $n \geq 3$  cosine parameterization scenarios.

The paper is organized as follows. In Sec.II, we consider the Mukhanov-Sasaki equation with double oscillation of the sound speed parameterization and we solve it numerically obtaining the power spectrum of the comoving curvature perturbation. Then, in Sec.III A, we show the energy spectra of secondary GWs induced by the primordial scalar sources during the inflationary and RD eras, for various parameter sets respectively. Considering ongoing and forthcoming GW experiments, we study the phenomenological implications on induced GWs from both inflationary and RD epochs in Sec.IV. Finally, we conclude with final comments and discussions in Sec.V.

## II. SOUND SPEED RESONANCE AND POWER SPECTRUM

Let us consider the Mukhanov-Sasaki equation in the Fourier space:

$$v_p'' + \left( c_s^2 p^2 - \frac{z''}{z} \right) v_p = 0, \quad (1)$$

where  $v''$  second derivatives with respect to the conformal time  $\tau$  with  $d\tau \equiv dt/a$ . As a convention we assume that  $\tau < 0$  corresponds to during inflation era and  $\tau > 0$  is at post-inflation. In MS equation we introduced the canonical variable  $v \equiv z\zeta$  where  $\zeta$  is the comoving curvature perturbation and  $z \equiv \sqrt{2\epsilon}a/c_s$ , with the Hubble slow-roll parameter  $\epsilon \equiv -\frac{1}{H^2} \frac{dH}{dt}$ . In dS approximation during inflation, the scale factor is  $a = e^{Ht}$  with constant  $H$ , which is equivalent to  $a = -1/(H\tau)$ ;  $c_s \equiv c_s(\tau)$  is the time varying sound speed. Notice that  $\epsilon$  is assumed to be time-independent and  $\epsilon \ll 1$  in this paper. Thus Eq.(1) corresponds to

$$v_p''(\tau) + \left( c_s^2 p^2 - \frac{2c_s'}{\tau c_s} - 2 \left( \frac{c_s'}{c_s} \right)^2 + \frac{c_s''}{c_s} - \frac{2}{\tau^2} \right) v_p(\tau) = 0. \quad (2)$$

In Ref. [70], it was proposed that the primordial density perturbations can be overly amplified in a narrow band through a modification with a single cosine function to the sound speed of the inflaton. As mentioned in the introduction, in this paper we generalize it to the scenario with the sound speed of a single inflaton with multi-oscillations as follows:

$$c_s^2 = 1 - 2 \sum_N \xi_{*N} [1 - \cos(2p_{*N}\tau)], \quad \tau_0 \leq \tau < 0, \quad (3)$$

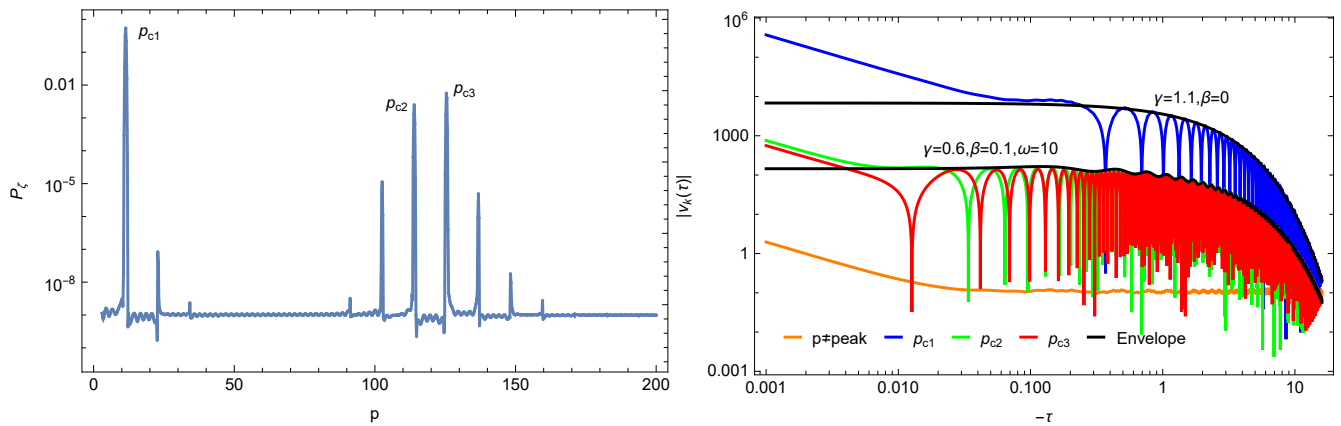


FIG. 1. The power spectrum of the comoving curvature perturbation  $P_\zeta(p)$  (Left), as a function of the peak value, and the absolute of  $v_p(\tau)$  solutions, as a function of conformal time  $\tau$ , for several resonating modes (Right) with parameter set  $p_{*1} = 10$ ,  $p_{*2} = 100$ ,  $\xi_{*1} = 0.1$ ,  $\xi_{*2} = 0.012$ ,  $\tau_0 = -16$ . In the left panel, two groups of peaks, one centering on  $p \sim 10$  and the other on  $p \sim 120$ , correspond to the sound speed resonances of characteristic oscillation modes with frequencies  $p_{*1}$  and  $p_{*2}$ , respectively. In the right panel, we display the  $v$  solutions corresponding to dominant peak(s) among each  $p_*$ -peak group, namely  $p_{c1}$  (blue),  $p_{c2}$  (green), and  $p_{c3}$  (red), which are indeed boosted comparing to the non-resonating mode with wave-number  $p \neq \text{peak}$  (orange). Interestingly, small oscillatory modulations are observed in the envelopes of  $|v_p|$  in  $p_{c2}$ - and  $p_{c3}$ -modes. The  $\gamma$ ,  $\beta$  and  $\omega$  are used to parameterize the resonating modes' envelopes given by Eq.(6).

where  $\xi_{*N}$  are small dimensionless parameters and  $p_{*N}$  are the oscillatory frequencies,  $N = 0, 1, 2, \dots$ , and  $\tau_0$  corresponds to the conformal time when oscillation effectively starts. In the following, we will consider the simplified case where the sum can be perturbatively truncated just to two harmonics as follows:

$$c_s^2 = 1 - 2\xi_{*1} [1 - \cos(2p_{*1}\tau)] - 2\xi_{*2} [1 - \cos(2p_{*2}\tau)], \quad \tau_0 \leq \tau < 0. \quad (4)$$

Notice that Eq.(4) reduces to the conventional case studied in Ref.[70] for vanishing  $\xi_{*2}$ . To have a positively definite  $c_s$ , we take  $0 \leq \xi_{*1,2} \lesssim 0.1$  in practice. The oscillation begins at  $\tau_0$ , when the characteristic  $p_{*1,2}$ -modes are well inside the Hubble radius, i.e.  $|\tau_0 p_{*1,2}| \gg 1$ . For simplicity, we assume that  $c_s$  can transit from unity to Eq.(4) smoothly at the start of the oscillation. Putting Eq.(4) into Eq.(2) and setting the mode function at the beginning of resonance to the Bunch-Davies vacuum  $v_p(\tau_0) = e^{-ip\tau_0}/\sqrt{2p}$ , one can numerically solve  $v_p(\tau)$  during inflation  $\tau_0 \leq \tau < 0$ .

With the rapid expansion during the inflation process, the perturbative  $p$ -mode will eventually exit the Hubble horizon, decohering the quantum fluctuation into the classical one. By the definition of dimensionless primordial power spectrum,  $P_\zeta \equiv p^3 |\zeta_p|^2 / (2\pi^2)$ , and the fact that it freezes at the super-horizon scale, we can rewrite  $P_\zeta$  in terms of  $v$  as

$$P_\zeta(p) = 2A_s p^3 |v_p(\tau_p)\tau_p|^2, \quad (5)$$

where  $\tau_p \simeq -1/(c_s p) \simeq -1/p$  is the sound horizon (approximate Hubble horizon) exiting time of the corresponding  $p$ -mode. Here,  $A_s = H^2/(8\pi^2\epsilon)$  is the amplitude of the power spectrum predicted by the conventional inflationary paradigm. From dimensional analysis, as we rescale  $p \rightarrow p/\alpha$ ,  $\tau \rightarrow \alpha\tau$  with constant  $\alpha$ , the  $p$ -mode scales as  $v_p \rightarrow \sqrt{\alpha}v_p$  and hence  $P_\zeta(p)$  remains the same as expected. Thus, all physical quantities, such as  $p$ ,  $\tau$  etc., can be rescaled to dimensional ones by considering  $\alpha$  as a dimensional quantity. We will restore the appropriate units for each quantity in Sec. IV for comparisons with experiments.

In Fig.1, we show a typical profile of the primordial power spectrum  $P_\zeta(p)$ , and  $v_p(\tau)$  solutions for several resonating modes. As a natural extend to the single cosine parameterization of  $c_s$  investigated in Refs.[7, 70], the presence of two characteristic frequencies in Eq.(4) results in two groups of narrow resonating peaks centering at  $\sim p_{*1}$  and  $p_{*2}$  in the  $P_\zeta(p)$  spectrum (see the left panel). In this sense, we simply define “ $p_{*1}$ -peak group” and “ $p_{*2}$ -peak group” as the peaks located around  $\sim p_{*1}$  and  $p_{*2}$  respectively. For the case in Fig.1, there is only one significant peak ( $p_{c1} \simeq 11$ ) in the  $p_{*1}$ -peak group and two dominant peaks ( $p_{c2} \simeq 114$  and  $p_{c3} \simeq 125$ ) in the  $p_{*2}$ -peak group, and the corresponding resonating modes are displayed in the right panel. One can see that, the non-resonating modes with  $p \neq \text{peak}$  evolve as usual in the Bunch-Davies state, whereas the resonating  $p_{c1}$ -,  $p_{c2}$ - and  $p_{c3}$ -modes enter in resonance on sub-horizon scales. Besides the similar resonance behavior as in Refs.[7, 70] (e.g.  $p_{c1}$ -mode), we find new small oscillatory modulations in the envelope of  $|v_p|$  of  $p_{c2}$ - and  $p_{c3}$ -modes, which are not found in the single cosine  $c_s$  case. The envelope of the resonating modes before Hubble-exiting can be effectively described by the following

profile:

$$|v_{p_{ci}}(\tau)| \propto e^{\frac{1}{2}\gamma_i \xi_i p_{ci}(\tau - \tau_0)} (1 - \beta_i \cos(2\omega_i(\tau - \tau_0))), \quad (6)$$

where  $p_{ci}$ -mode corresponds to the  $i$ -th peak of power spectrum. Here,  $\xi_i = \xi_{*1}$  ( $\xi_{*2}$ ) if the  $i$ -th peak belongs to  $p_{*1}$ - ( $p_{*2}$ -) peak group, and  $\gamma_i$  is the correction factor to fit the exponential growing magnitude of each resonating mode, which is practically  $\sim 1$  for the  $p_{*1}$ -peak group and  $\sim \mathcal{O}(0.1)$  for the  $p_{*2}$ -peak group. For the oscillatory modulation of the mode envelope, it can be well matched by setting  $\beta_i = \xi_{*1}, \omega_i = p_{*1}$  for the  $p_{*2}$ -peak group and  $\beta_i = 0$  for  $p_{*1}$ -peak group. It is worth to mention that such oscillatory envelope modulation of the resonating modes is also observed in Ref.[24], where the parametric resonance arises from a periodic structure superposing on the slow-roll inflation potential. Let us comment more on the appearance of the oscillatory behavior in the envelope of the resonating mode in  $p_{*2}$ -peak group. We focus on the mode  $v_p(\tau)$  with  $p \sim p_{*2}$  and in the subhorizon regime  $|p\tau| \gg 1$ . Combining Eqs. (2) and (4) and assuming  $p_{*1} \ll p_{*2}$  and  $\xi_{*1} \gg \xi_{*2}$  (for most cases studied in the paper), we obtain  $v_p''(\tau) + ((p^2 - 2p^2\xi_{*1} + 2p^2\xi_{*1}\cos(2p_{*1}\tau)) + (2p^2\xi_{*2} - 4p_{*2}^2\xi_{*2})\cos(2p_{*2}\tau))v_p(\tau) = 0$ . It is easy to check that in single oscillation case with  $p_{*1} = p_{*2} = p_*$ , the above equation reduces to the standard Mathieu equation  $v_p''(\tau) + (\tilde{b} + \tilde{q}\cos(2p_*\tau))v_p(\tau) = 0$ , where  $\tilde{b}$  and  $\tilde{q}$  are independent of  $\tau$ . Whereas in the double oscillation case, the term  $b \equiv p^2 - 2p^2\xi_{*1} + 2p^2\xi_{*1}\cos(2p_{*1}\tau)$  depends on the variable  $\tau$ , so the aforementioned equation is not the Mathieu equation and can not be solved analytically. However, compared to the high-frequency oscillation term  $\cos(2p_{*2}\tau)$ , the term  $\cos(2p_{*1}\tau)$  oscillates much slower in frequency  $p_{*1}$ , indicating a slowly varying  $b$  with respect to  $\tau$ . Such a slow oscillatory factor in Mathieu-like equation provides a clue to understand the appearance of the oscillatory modulation with the certain frequency  $p_{*1}$  in the envelope of the resonating mode in  $p_{*2}$ -peak group.

In Fig.2, we display the power spectra of the curvature perturbations for different parameter combinations which satisfy the perturbative condition  $P_\zeta < 1$ . In particular, the  $\xi_{*2} = 0$  case reduces to the conventional resonance pattern predicted in Refs.[7, 70] with only one dominant peak  $p_{c1} \sim p_{*1}$  and several subdominant peaks in the tail of the power spectrum. As we turn on  $\xi_{*2}$ , there appears two groups of narrow resonating peaks centering on around  $p_{*1}$  and  $p_{*2}$ . Moreover, much more peaks can present in the  $p_{*2}$ -peak group for relatively large ratio  $p_{*2}/p_{*1}$  (see the lower panels). As we will see later, the energy density of induced GWs is related to the scalar power spectrum as  $\Omega_{GW} \sim \int \int P_\zeta^2 \sim \int \int v^4$  from dimensional scaling, thus the sub-dominant peaks are more than one order of magnitude less than the most dominant peak in each  $p_*$ -peak group, giving negligible contributions to the GW spectrum. Hence we refer the ‘‘dominant’’ peaks to those in the same order of amplitude of the highest peak in each  $p_*$ -peak group, which are exclusively labeled for different cases in Fig.2. One can see that, except some extreme cases like vanishing  $\xi_{*2}$  or small  $p_{*1}\tau_0$  (see Fig.8), there is generically only one dominant peak in the  $p_{*1}$ -peak group and one/several dominant peak(s) in the  $p_{*2}$ -peak group.

From the resonance effect, the peaks of the power spectrum are narrow and sharp and the power spectrum can be approximated as sum of Dirac-delta functions

$$P_\zeta(p) \simeq A_s \left( 1 + \sum_{i=1}^n \frac{1}{2} A_i \xi_i p_{ci} \delta(p - p_{ci}) \right). \quad (7)$$

Here,  $A_i$  is the magnitude of the amplification of the  $i$ -th resonating mode and the combination  $A_s A_i$  can be seen as the amplitude of peak’s height. Actually,  $A_i$  is reminiscent of the exponential parameterization of the power spectrum considered in Refs.[7, 70]. Indeed,  $\xi_i p_{ci}$  is determined by estimating the area of the peak with a triangle approximation, which can be interpreted as the width of the corresponding peak.

### III. INDUCED GRAVITATIONAL WAVES IN EARLY UNIVERSE

It is expected that the primordial density perturbations enhanced by the narrow sound speed resonance can induce large GW signals according to the second-order cosmological perturbation theory. In this section, we provide theoretical analyses of the stochastic GW background induced by the resonating modes of primordial density perturbations during the inflationary and RD eras.

#### A. Radiation Dominated Era

Let us compute the second-order tensor modes generated from the first-order scalar perturbation with the same standard approach considered in Refs. [4, 12, 13]. In absence of anisotropy in the stress-energy tensor, the perturbed

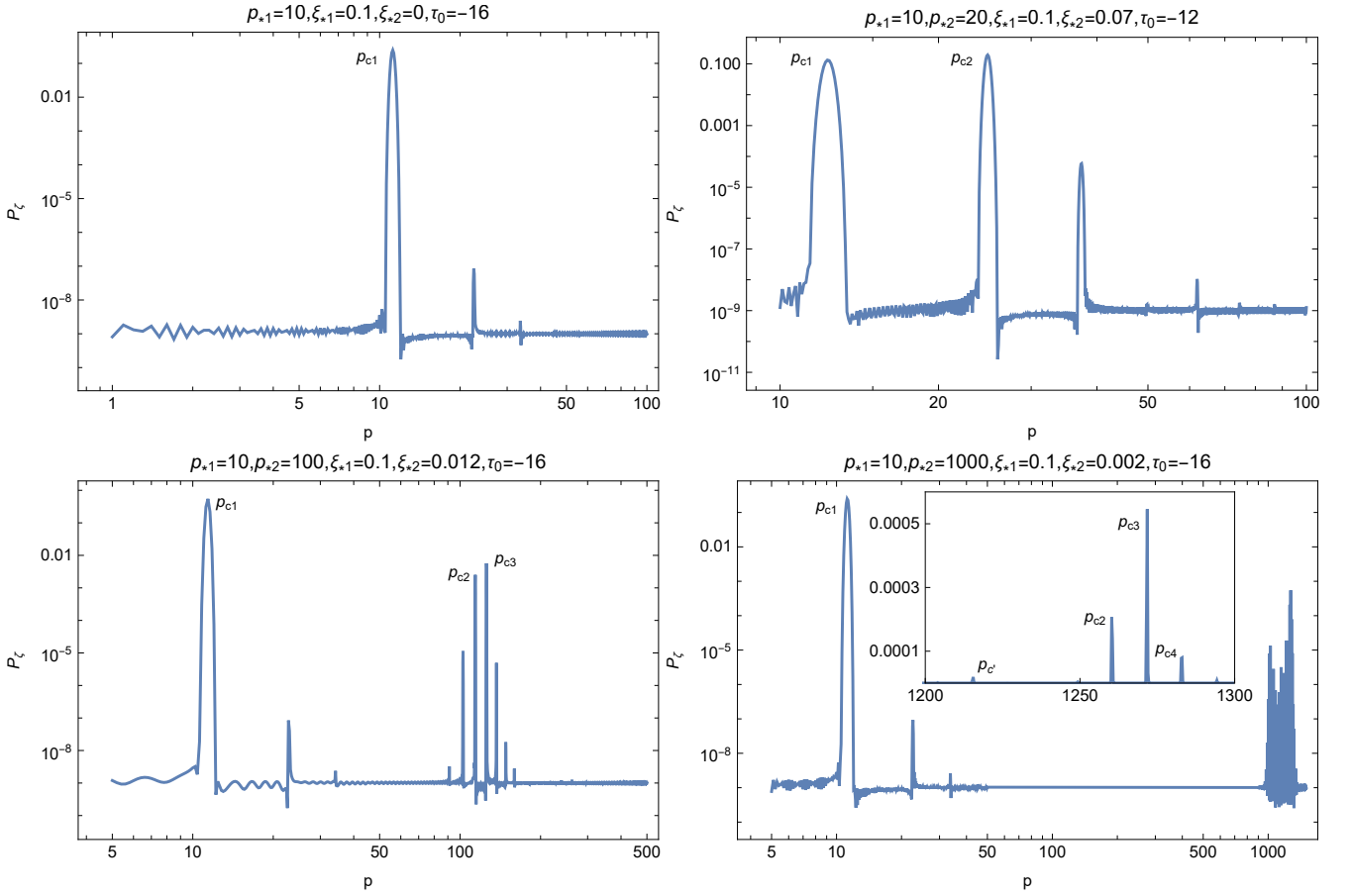


FIG. 2. The power spectrum of the curvature perturbation in  $(P_\zeta, p)$  plane for different parameters. The height of all peaks in  $P_\zeta(p)$  should be no more than the unity in order to respect the perturbative bound. In the upper-left panel, the case with vanishing  $\xi_{*2}$  shows the conventional resonance pattern of single cosine parameterization of  $c_s$ . In the cases with non-vanishing  $\xi_{*1}$  and  $\xi_{*2}$ , there can appear much more peaks in the  $p_{*2}$ -peak group, especially for relatively large ratio  $p_{*2}/p_{*1}$ . We define the dominant resonance peaks as those that are in the same order of amplitude of the highest peak in each  $p_*$ -peak group, and use  $p_{ci}$  to denote the  $i$ -th dominant peak. Generically, one dominant peak is found in the  $p_{*1}$ -peak group and one/several dominant peak(s) in the  $p_{*2}$ -peak group. Moreover, the subdominant resonance  $p_{c'}$ -peak in the lower-right panel gives a negligible contribution to the energy density of induced GWs, as we will see later.

metric in the conformal Newtonian gauge reads

$$d^2s = a^2(\tau) \left\{ -(1 - 2\Phi(\tau, \mathbf{x}))d\tau^2 + \left[ (1 + 2\Phi(\tau, \mathbf{x}))\delta_{ij} + \frac{1}{2}h_{ij}(\tau, \mathbf{x}) \right] dx^i dx^j \right\}, \quad (8)$$

where  $\Phi(\tau, \mathbf{x})$  is the Bardeen potential in first order, and  $h_{ij}(\tau, \mathbf{x})$  is transverse and traceless second-order tensor mode satisfying  $\delta^{ij}h_{ij} = 0$  and  $\delta^{ij}\partial_i h_{jk} = 0$ . We define the Fourier transform of GW tensor  $h_{ij}(\tau, \mathbf{x})$  as

$$h_{ij}(\tau, \mathbf{x}) \equiv \sum_{\lambda=+, \times} \int \frac{d^3\mathbf{k}}{(2\pi)^3} e^{i\mathbf{k}\cdot\mathbf{x}} h_{\mathbf{k}}^\lambda(\tau) e_{ij}^\lambda(\mathbf{k}), \quad (9)$$

where  $\lambda = +, \times$  denote the polarizations of the GWs. The two time-independent polarization tensors  $e_{ij}^\lambda(\mathbf{k})$  are expressed in terms of orthonormal basis vectors  $e_i(\mathbf{k}), \bar{e}_i(\mathbf{k})$  perpendicular to  $\mathbf{k}$ ,

$$\begin{aligned} e_{ij}^\times(\mathbf{k}) &\equiv \frac{1}{\sqrt{2}} [e_i(\mathbf{k})\bar{e}_j(\mathbf{k}) + \bar{e}_i(\mathbf{k})e_j(\mathbf{k})], \\ e_{ij}^+(\mathbf{k}) &\equiv \frac{1}{\sqrt{2}} [e_i(\mathbf{k})e_j(\mathbf{k}) - \bar{e}_i(\mathbf{k})\bar{e}_j(\mathbf{k})]. \end{aligned} \quad (10)$$

Sourced by the scalar perturbation  $S_{lm}(\tau, \mathbf{x})$ , the equation of motion for the induced GWs at second order reads

$$h''_{ij}(\tau, \mathbf{x}) + 2\mathcal{H}h'_{ij}(\tau, \mathbf{x}) - \nabla^2 h_{ij}(\tau, \mathbf{x}) = -4\hat{T}_{ij}^{lm} S_{lm}(\tau, \mathbf{x}), \quad (11)$$

where the projector  $\hat{T}_{ij}^{lm}$  selects the transverse and traceless parts of the source term  $\hat{T}_{ij}^{lm} S_{lm}(\tau, \mathbf{x}) \equiv \sum_{\lambda} \int \frac{d^3 \mathbf{k}}{(2\pi)^3} e^{i\mathbf{k}\cdot\mathbf{x}} e_{ij}^{\lambda}(\mathbf{k}) e_{lm}^{\lambda}(\mathbf{k}) S_{lm}(\tau, \mathbf{k})$ . In the momentum space, we have

$$h_{\mathbf{k}}^{\lambda''}(\tau) + 2\mathcal{H}h_{\mathbf{k}}^{\lambda'}(\tau) + k^2 h_{\mathbf{k}}^{\lambda}(\tau) = S_{\mathbf{k}}^{\lambda}(\tau) \quad (12)$$

with  $S_{\mathbf{k}}^{\lambda}(\tau) \equiv -4e_{lm}^{\lambda}(\mathbf{k}) S_{lm}(\tau, \mathbf{k})$ . The solution for the GWs can be obtained by using Green's function method,

$$h_{\mathbf{k}}^{\lambda}(\tau) = \frac{1}{a(\tau)} \int^{\tau} d\tau_1 a(\tau_1) g_{\mathbf{k}}(\tau, \tau_1) S_{\mathbf{k}}^{\lambda}(\tau_1), \quad (13)$$

where the Green function  $g_{\mathbf{k}}(\tau, \tau_1)$  in RD era is

$$g_{\mathbf{k}}(\tau, \tau_1) = \frac{1}{k} \sin(k\tau - k\tau_1) \Theta(\tau - \tau_1) \quad (14)$$

with the Heaviside step function  $\Theta(\tau - \tau_1)$ . The source term during the RD era is given by

$$\mathcal{S}_{ij}(\tau, \mathbf{x}) = 4\Phi\partial_i\partial_j\Phi(\tau, \mathbf{x}) + \partial_i\Phi\partial_j\Phi(\tau, \mathbf{x}) - 2\mathcal{H}^{-1}\partial_i\Phi\partial_j\Phi'(\tau, \mathbf{x}) - \mathcal{H}^{-2}\partial_i\Phi'\partial_j\Phi'(\tau, \mathbf{x}), \quad (15)$$

where  $\mathcal{H} \equiv a'/a$  is the comoving Hubble parameter related to  $H$  by  $\mathcal{H} = aH$ . Then from the definition of  $S_{\mathbf{k}}^{\lambda}(\tau)$ , we obtain

$$S_{\mathbf{k}}^{\lambda}(\tau) = 4 \int \frac{d^3 \mathbf{p}}{(2\pi)^3} e^{\lambda}(\mathbf{k}, \mathbf{p}) [3\Phi_{\mathbf{p}}(\tau)\Phi_{\mathbf{k}-\mathbf{p}}(\tau) + \mathcal{H}^{-2}\Phi'_{\mathbf{p}}(\tau)\Phi'_{\mathbf{k}-\mathbf{p}}(\tau) + \mathcal{H}^{-1}\Phi'_{\mathbf{p}}(\tau)\Phi_{\mathbf{k}-\mathbf{p}}(\tau) + \mathcal{H}^{-1}\Phi_{\mathbf{p}}(\tau)\Phi'_{\mathbf{k}-\mathbf{p}}(\tau)], \quad (16)$$

where  $e^{\lambda}(\mathbf{k}, \mathbf{p}) \equiv e_{ij}^{\lambda}(\mathbf{k}) p_i p_j$  take the explicit form  $e^{+}(\mathbf{k}, \mathbf{p}) = p^2 \sin^2 \theta \cos 2\varphi / \sqrt{2}$  and  $e^{\times}(\mathbf{k}, \mathbf{p}) = p^2 \sin^2 \theta \sin 2\varphi / \sqrt{2}$  [7, 82, 83]. Here,  $\mathbf{k}$  and  $\mathbf{p}$  are respectively the wave vector of the induced GWs and the perturbed source, and  $(p, \theta, \varphi)$  are the spherical coordinates of  $\mathbf{p}$  in system whose  $(\hat{x}, \hat{y}, \hat{z})$  axes are aligned with  $(\mathbf{e}(\mathbf{k}), \bar{\mathbf{e}}(\mathbf{k}), \mathbf{k})$ . During the RD epoch, the relation between Barden potential  $\Phi_{\mathbf{p}}(\tau)$  and the comoving curvature perturbation  $\zeta_{\mathbf{p}}$  is [12, 84]

$$\Phi_{\mathbf{p}}(\tau) = \frac{2}{3} T(p\tau) \zeta_{\mathbf{p}}, \quad (17)$$

with transfer function given by

$$T(p\tau) = \frac{9}{(p\tau)^2} \left[ \frac{\sin(p\tau/\sqrt{3})}{p\tau/\sqrt{3}} - \cos(p\tau/\sqrt{3}) \right]. \quad (18)$$

Putting Eqs.(17)-(18) into Eq.(16), one can express the source in terms of the primordial perturbation as

$$S_{\mathbf{k}}^{\lambda}(\tau) = \frac{16}{9} \int \frac{d^3 \mathbf{p}}{(2\pi)^3} e^{\lambda}(\mathbf{k}, \mathbf{p}) f(\mathbf{k}, \mathbf{p}, \tau) \zeta_{\mathbf{p}} \zeta_{\mathbf{k}-\mathbf{p}}, \quad (19)$$

$$f(\mathbf{k}, \mathbf{p}, \tau) \equiv 3T(p\tau)T(|\mathbf{k}-\mathbf{p}|\tau) + \mathcal{H}^{-2}T'(p\tau)T'(|\mathbf{k}-\mathbf{p}|\tau) + \mathcal{H}^{-1}T'(p\tau)T(|\mathbf{k}-\mathbf{p}|\tau) + \mathcal{H}^{-1}T(p\tau)T'(|\mathbf{k}-\mathbf{p}|\tau),$$

where the prime here still denotes the derivative with respect to  $\tau$ .

On the other hand, the correlator for tensor metric perturbation is defined as

$$\langle \hat{h}_{\mathbf{k}}^{\lambda}(\tau) \hat{h}_{\mathbf{k}'}^s(\tau) \rangle = (2\pi)^3 \delta^{\lambda s} \delta^{(3)}(\mathbf{k} + \mathbf{k}') \frac{2\pi^2}{k^3} P_h(k, \tau), \quad (20)$$

where  $\hat{h}_{\mathbf{k}}$  represents the operator associated with the GW  $\mathbf{k}$ -mode by canonical quantization, and  $P_h(k, \tau)$  is the dimensionless power spectrum for the GWs of each polarization. Combining Eqs.(13),(14),(19), the GW two-point correlator can be expressed by the primordial four-point correlator,

$$\langle \hat{h}_{\mathbf{k}}^{\lambda}(\tau) \hat{h}_{\mathbf{k}'}^s(\tau) \rangle = \frac{1}{a^2(\tau)} \int^{\tau} d\tau_1 \int^{\tau} d\tau_2 g_{\mathbf{k}}(\tau, \tau_1) g_{\mathbf{k}}(\tau, \tau_2) a(\tau_1) a(\tau_2) \times \left( \frac{16}{9} \right)^2 \int \frac{d^3 \mathbf{p}}{(2\pi)^3} e^{\lambda}(\mathbf{k}, \mathbf{p}) f(\mathbf{k}, \mathbf{p}, \tau_1) \int \frac{d^3 \mathbf{q}}{(2\pi)^3} e^s(\mathbf{k}', \mathbf{q}) f(\mathbf{k}', \mathbf{q}, \tau_2) \langle \hat{\zeta}_{\mathbf{p}} \hat{\zeta}_{\mathbf{k}-\mathbf{p}} \hat{\zeta}_{\mathbf{q}} \hat{\zeta}_{\mathbf{k}'-\mathbf{q}} \rangle. \quad (21)$$



Assuming the Gaussianity of the curvature perturbation, one can use the Wick theorem and the definition of the dimensionless power spectrum of  $\zeta_{\mathbf{p}}$ ,

$$\langle \hat{\zeta}_{\mathbf{p}}(\tau) \hat{\zeta}_{\mathbf{p}'}(\tau) \rangle = (2\pi)^3 \delta^{(3)}(\mathbf{p} + \mathbf{p}') \frac{2\pi^2}{p^3} P_{\zeta}(p, \tau), \quad (22)$$

to rewrite Eq.(21) as

$$\begin{aligned} \langle \hat{h}_{\mathbf{k}}^{\lambda}(\tau) \hat{h}_{\mathbf{k}'}^s(\tau) \rangle &= \delta^{\lambda s} (2\pi)^3 \delta^{(3)}(\mathbf{k} + \mathbf{k}') \left( \frac{16}{9} \right)^2 \frac{1}{a^2(\tau)} \int^{\tau} d\tau_1 \int^{\tau} d\tau_2 g_{\mathbf{k}}(\tau, \tau_1) g_{\mathbf{k}}(\tau, \tau_2) a(\tau_1) a(\tau_2) \\ &\times \int \frac{d^3\mathbf{p}}{(2\pi)^3} e^{\lambda}(\mathbf{k}, \mathbf{p}) e^s(\mathbf{k}, \mathbf{p}) f(\mathbf{k}, \mathbf{p}, \tau_1) f(\mathbf{k}, \mathbf{p}, \tau_2) \frac{2\pi^2}{p^3} \frac{2\pi^2}{|\mathbf{k} - \mathbf{p}|^3} P_{\zeta}(p) P_{\zeta}(|\mathbf{k} - \mathbf{p}|). \end{aligned} \quad (23)$$

Plugging the expressions for  $e^{\lambda}(\mathbf{k}, \mathbf{p})$ ,  $g_{\mathbf{k}}(\tau, \tau_1)$  (Eq.(14)) and  $f(\mathbf{k}, \mathbf{p}, \tau)$  (Eq.(19)) into Eq.(23), and introducing three dimensionless variables  $u = |\mathbf{k} - \mathbf{p}|/k$ ,  $v = p/k$  and  $z = k\tau$ , we obtain the power spectrum of the induced GWs after a straightforward and tedious calculation [7, 12, 13, 15, 83, 85, 86]

$$\begin{aligned} P_h^{RD}(k, \tau) &= \int_0^{\infty} dv \int_{|v-1|}^{(v+1)} du \left( \frac{4v^2 - (1 + v^2 - u^2)^2}{4uv} \right)^2 P_{\zeta}(vk) P_{\zeta}(uk) \\ &\times \frac{4}{81} \frac{1}{z^2} (\cos^2 z \mathcal{I}_c^2(u, v, z) + \sin^2 z \mathcal{I}_s^2(u, v, z) + \sin 2z \mathcal{I}_c(u, v, z) \mathcal{I}_s(u, v, z)), \end{aligned} \quad (24)$$

with the long expressions  $\mathcal{I}_c$  and  $\mathcal{I}_s$  given by

$$\begin{aligned} \mathcal{I}_c(u, v, z) &= 4 \int^z d\tilde{z} (-\tilde{z} \sin \tilde{z}) (2T(v\tilde{z})T(u\tilde{z}) + (T(v\tilde{z}) + v\tilde{z}T_{,1}(v\tilde{z})) (T(u\tilde{z}) + u\tilde{z}T_{,1}(u\tilde{z}))), \\ \mathcal{I}_s(u, v, z) &= 4 \int^z d\tilde{z} (\tilde{z} \cos \tilde{z}) (2T(v\tilde{z})T(u\tilde{z}) + (T(v\tilde{z}) + v\tilde{z}T_{,1}(v\tilde{z})) (T(u\tilde{z}) + u\tilde{z}T_{,1}(u\tilde{z}))). \end{aligned} \quad (25)$$

Note that  $T_{,1}(x) \equiv dT(x)/dx$  for any variable  $x$ .

With the expansion of the universe, the induced GWs eventually evolve into a stochastic background which can be characterized by the energy density fraction  $\Omega_{\text{GW}}(\tau, k)$ , which only depends on the magnitude of the wave vector  $\mathbf{k}$ . When the relevant GW mode is well inside the Hubble horizon during the RD era, the GW energy density fractions related to its power spectrum as

$$\Omega_{\text{GW}}^{RD}(\tau, k) = \frac{1}{24} \left( \frac{k}{\mathcal{H}} \right)^2 \overline{P_h^{RD}(\tau, k)}, \quad (26)$$

where the two polarization modes have been summed over, and the overline means the time average over several periods of the GWs [83, 87, 88]. Note that  $\mathcal{H}(\tau) \simeq 1/\tau$  in RD epoch. To compare with the experiments, the current abundance of GW energy spectrum is estimated as

$$\begin{aligned} \Omega_{\text{GW}}(\tau_0, k) h_0^2 &= c_g \Omega_{r,0} \Omega_{\text{GW}}^{RD}(\tau_f, k) h_0^2 \\ &= \frac{h_0^2 c_g \Omega_{r,0}}{972} \int_0^{\infty} dv \int_{|v-1|}^{(v+1)} du \left( \frac{4v^2 - (1 + v^2 - u^2)^2}{4uv} \right)^2 P_{\zeta}(vk) P_{\zeta}(uk) (\mathcal{I}_c^2(u, v, k\tau_f) + \mathcal{I}_s^2(u, v, k\tau_f)), \end{aligned} \quad (27)$$

where the expressions of  $\mathcal{I}_c$  and  $\mathcal{I}_s$  are given in Eq. (25). Here,  $\tau_f$  represents the end of the RD era when  $k\tau_f \gg \mathcal{O}(10^3)$  for most of the GW  $k$ -mode of interest. In fact, as discussed in [83], the upper and lower limits in the integration of  $\mathcal{I}_c$  and  $\mathcal{I}_s$  can be safely set to 1 and  $+\infty$ , thus we use  $\mathcal{I}_{s,c}(u, v, +\infty) \equiv \mathcal{I}_{s,c}(u, v)$  for simplicity in the followings. We take the present reduced dimensionless Hubble parameter  $h_0 \simeq 0.7$ , radiation energy density fraction  $\Omega_{r,0} \simeq 5.4 \times 10^{-5}$  and the factor  $c_g \simeq 0.4$  [83, 85, 89].

For the source power spectrum Eq.(7) generated by the narrow parametric resonance of the double cosine parameterization of the sound speed Eq.(4), we obtain the corresponding GW energy spectrum

$$\begin{aligned} \Omega_{\text{GW}}(\tau_0, k) h_0^2 &= \frac{h_0^2 c_g \Omega_{r,0} A_s^2}{3888} \sum_{i=1}^n \sum_{j=1}^n A_i A_j \xi_i \xi_j \frac{p_{ci}}{k} \frac{p_{cj}}{k} \left( \frac{4p_{cj}^2 k^2 - (k^2 + p_{cj}^2 - p_{ci}^2)^2}{4p_{ci} p_{cj} k^2} \right)^2 \\ &\times \left( \mathcal{I}_c^2\left(\frac{p_{ci}}{k}, \frac{p_{cj}}{k}\right) + \mathcal{I}_s^2\left(\frac{p_{ci}}{k}, \frac{p_{cj}}{k}\right) \right) \Theta(p_{ci} - |p_{cj} - k|) \Theta(p_{cj} + k - p_{ci}), \end{aligned} \quad (28)$$



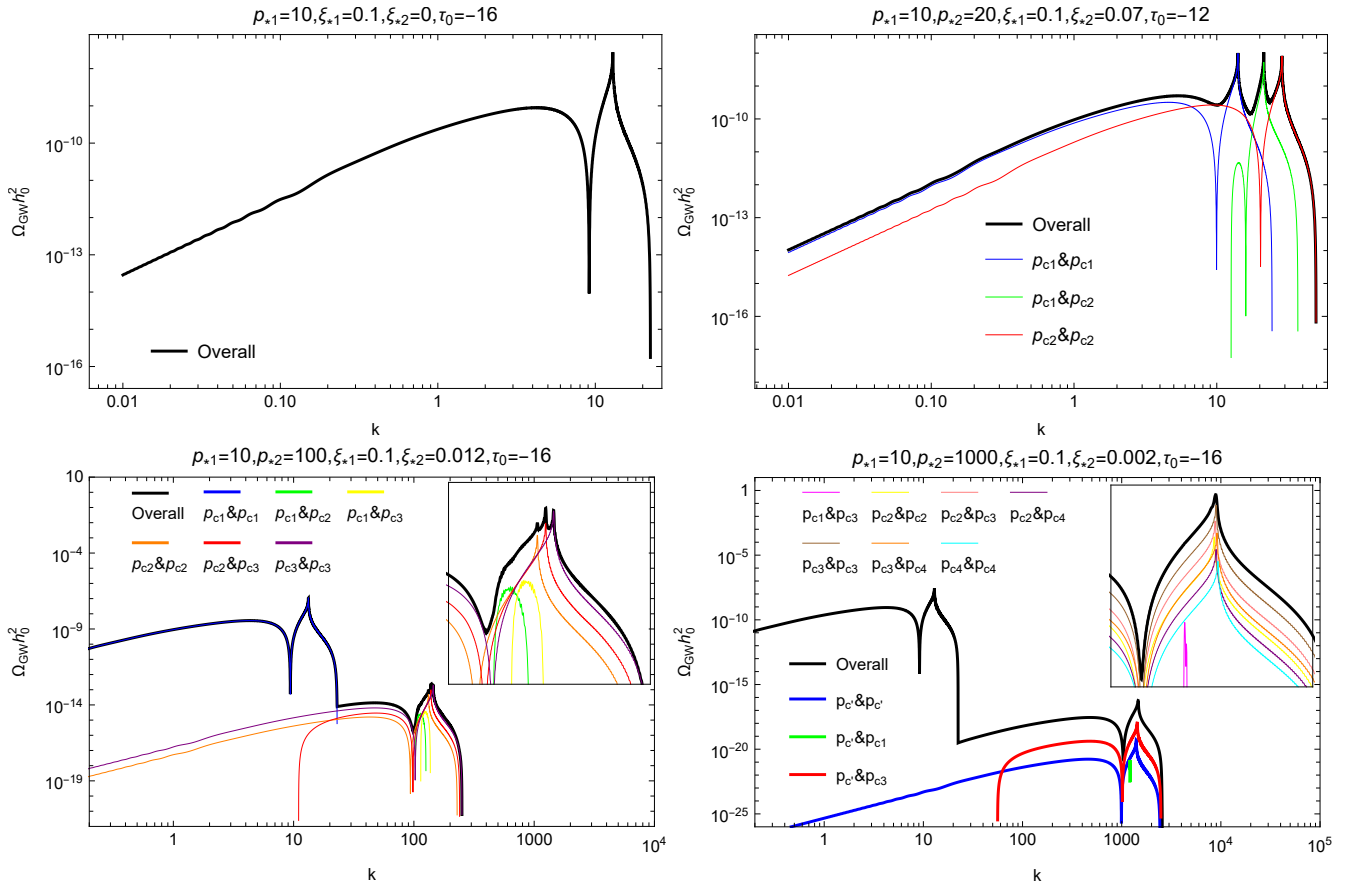


FIG. 3. The energy spectrum of GWs induced during RD epoch corresponding to the source spectrum in Fig.2. The black line denotes the overall magnitude of the GW energy spectrum, and the other colored lines denote the component decomposition generated by the convolution of dominant  $p_{ci}$ - and  $p_{cj}$ -peaks (see Eq.(28)). The typical profile of the GW spectrum is reproduced in the single cosine parameterization of  $c_s$ , as displayed in the upper-left panel. For the double cosine scenario, the induced GW spectrum composite of at least two major peaks. Moreover, the multiple dominant peaks in  $p_{*2}$ -peak group of source spectrum can give rise to the localized fine feature with sharp spikes to the induced GW spectrum (for instance, see inset in the lower-left panel). In the lower-right panel, one can see that the contribution to the GW energy from the subdominant resonating  $p_{c'}$ -peak (see the lower-right panel in Fig.2) can be safely neglected, indicating that only dominant peaks shall be taken into account.

where  $i, j = 1, \dots, n$  indices correspond to the resonant peaks in source spectrum. The  $P_\zeta < 1$  condition implies  $P_h < 1$  or equivalently  $\Omega_{\text{GW}}(\tau_0, k)h_0^2 \lesssim 10^{-6}$ , for the validity of the perturbative analysis.

In Fig.3, we display the overall induced GWs in RD era for different parameter sets, as well as the decomposition of each individual component corresponding to the convolution of dominant  $p_{ci}$ - and  $p_{cj}$ -peaks in Eq.(28). In principle, all peaks in source spectrum  $P_\zeta(p)$  shall be accounted, while in practice we only need to focus on the dominant peaks, such as  $p_{c1}, p_{c2}$  etc. as shown in Fig.2. Indeed the sub-dominant peaks generate negligible contributions to the overall energy density of the induced GWs. As shown in the the lower-right panel, the GW spectrum components involved with the sub-dominant peak  $p_{c'}$  (see the lower-right panel in Fig.2) are at least two orders of magnitude less than the overall GW spectrum. For the case with vanishing  $\xi_{*2}$  in the upper-left panel, we reproduce the conventional single-peak GW spectrum with a sharp peak at  $\simeq p_{*1}$  since only one dominant peak is in source spectrum (see the upper-left panel in Fig.2). When we turn on the second oscillatory mode with non-vanishing  $\xi_{*2}$ , there exist richer patterns in GW profile governed by the amplitude and position of multiple dominant peaks in  $P_\zeta$ . As argued in [26, 86], the  $n$   $p_{ci}$ -peaks ( $i = 1, 2, \dots, n$ ) in scalar source spectrum can generate at most  $n(n+1)/2$  peaks located in  $(p_{ci} + p_{cj})/\sqrt{3}$  in the induced GW spectrum. In particular, two dominant peaks with nearly equal height in source spectrum (see the upper-right panel in Fig. 2) are expected to yield three peaks at around  $p_{c1}, (p_{c1} + p_{c2})/2$  and  $p_{c2}$  in the GW spectrum, as shown in the upper-right panel in Fig.3. For the cases with relatively large ratio  $p_{*2}/p_{*1}$ , two broad principle peak-like structures at  $\simeq p_{*1}$  and  $\simeq p_{*2}$  are observed in GW spectrum, which are related to the presence of  $p_{*1}$ - and  $p_{*2}$ -peak groups in source spectrum, respectively (see the lower panels in Figs.2 and 3 for a direct comparison). Since the dominant peaks at  $p_{*2}$ -peak group are at  $2 \div 3$  orders of magnitude less than the dominant

one in  $p_{*1}$ -peak group, the magnitude of the induced GW spectrum peak(s) at  $\simeq p_{*2}$  is less than the peak at  $\simeq p_{*1}$  of around 10 orders. Moreover, when one zooms in the GW band at  $\simeq p_{*2}$ , the principle peak-like configuration can admit the localized fine structure with several narrow peaks originated from the intersection of multiple dominant peaks of source spectrum. Nevertheless, the appearance of such fine structure is highly sensitive to the specific amplitudes and positions of the resonating peaks in  $P_\zeta$  (see the insets in lower panels in Fig.3).

## B. Inflationary Era

Now let us investigate the GWs induced by the boosted curvature perturbations from sound speed resonances during the inflationary era. Due to the narrow resonance effect, GWs can be induced by the perturbed inflaton  $\delta\phi$  and its anisotropic stress [6, 7, 88, 90] as

$$\mathcal{S}_{ij}(\tau, \mathbf{x}) = \frac{c_s^2(\tau)}{M_p^2} \partial_i \delta\phi(\tau, \mathbf{x}) \partial_j \delta\phi(\tau, \mathbf{x}). \quad (29)$$

In the momentum space, the effective source term in Eq.(12) becomes

$$S_{\mathbf{k}}^\lambda(\tau) = -4 \frac{c_s^2(\tau)}{M_p^2} \int \frac{d^3\mathbf{p}}{(2\pi)^3} e^{i\lambda(\mathbf{k}, \mathbf{p})} \delta\phi_{\mathbf{p}}(\tau) \delta\phi_{\mathbf{k}-\mathbf{p}}(\tau). \quad (30)$$

Performing the standard procedure as that in RD era, we first write down the solution for the GW tensor mode in a more convenient way

$$h_{\mathbf{k}}^\lambda(\tau) = \int^\tau d\tau_1 g_{\mathbf{k}}(\tau, \tau_1) S_{\mathbf{k}}^\lambda(\tau_1), \quad (31)$$

where the Green function  $g_{\mathbf{k}}(\tau, \tau_1)$  during inflationary era is given by [90]

$$g_{\mathbf{k}}(\tau, \tau_1) = \frac{1}{2k^3\tau_1^2} e^{-ik(\tau+\tau_1)} (e^{2ik\tau}(1-ik\tau)(-i+k\tau_1) + e^{2ik\tau_1}(1+ik\tau)(i+k\tau_1)) \Theta(\tau - \tau_1). \quad (32)$$

The GW correlator  $\langle \hat{h}_{\mathbf{k}}^\lambda(\tau) \hat{h}_{\mathbf{k}'}^s(\tau) \rangle$  involves the unequal-time four-point correlation function  $\langle \delta\hat{\phi}_{\mathbf{p}}(\tau_1) \delta\hat{\phi}_{\mathbf{k}-\mathbf{p}}(\tau_1) \delta\hat{\phi}_{\mathbf{q}}(\tau_2) \delta\hat{\phi}_{\mathbf{k}'-\mathbf{q}}(\tau_2) \rangle$ , which is calculated in details in Ref.[91–93]. Finally, from Eq.(20), we obtain the following expression for the power spectrum [6, 8, 10]:

$$P_h^{\text{Inf}}(\tau, k) = 128 A_s^2 \epsilon^2 k^3 \int \sin^5 \theta d\theta \int p^6 dp \left| \int_{\tau_i}^\tau d\tau_1 g_{\mathbf{k}}(\tau, \tau_1) \tau_1^2 c_s^4(\tau_1) v_p(\tau_1) v_{|\mathbf{k}-\mathbf{p}|}(\tau_1) \right|^2, \quad (33)$$

where we have used the relation  $v_p = -\frac{1}{c_s M_p H \tau} \delta\phi_p$  in the spatially flat gauge. As in [7], the phase space integral  $\int p^2 \sin \theta d\theta dp$  can be integrated out using the thin ring approximation thanks to the narrow resonance effect. More precisely, the major contribution to  $P_h^{\text{Inf}}$  comes from the quite narrow resonant regime in the neighborhood of the overly amplified  $p_{ci}$ -mode (see Fig.2); so it is reasonable to set  $v_p = v_{p_{ci}}$  for  $p \in (p - \frac{1}{2}\xi_i p_{ci}, p + \frac{1}{2}\xi_i p_{ci})$  and  $v_p = 0$  otherwise. Then the geometric interpretation of the available phase space integral is the volume of the ringlike intersection of two spheres:  $i(j)$ -sphere with radius  $p_{ci}(p_{cj})$  and thickness  $\xi_i p_{ci}(\xi_j p_{cj})$ , and the distance of centers of  $i$ -sphere and  $j$ -sphere is  $k$  satisfying  $|p_{ci} - p_{cj}| < k < p_{ci} + p_{cj}$ . We adopt a simple approximation of the volume of such intersect configuration as  $\Delta\Pi_{ij} \simeq 2\pi p_{ci} \sin \theta_{ij} \xi_i p_{ci} \xi_j p_{cj}$  with  $\theta_{ij}$  given by  $\cos \theta_{ij} = (p_{ci}^2 + k^2 - p_{cj}^2)/(2p_{ci}k)$ . Taking all dominant peaks of  $P_\zeta$  into account, we obtain the induced GW power spectrum at the end of inflation  $\tau \simeq 0$ ,

$$P_h^{\text{Inf}}(\tau \simeq 0, k) \simeq A_s^2 \epsilon^2 \frac{16}{\pi k^3} \sum_{i=1}^n \sum_{j=1}^n \Delta\Pi_{ij} \left( 1 - \left( \frac{p_{ci}^2 + k^2 - p_{cj}^2}{2p_{ci}k} \right)^2 \right)^2 p_{ci}^4 \Theta(p_{ci} + p_{cj} - k) \Theta(k - |p_{ci} - p_{cj}|) \\ \times \left| \int_{\tau_0}^0 d\tau_1 e^{-ik\tau_1} ((-i + k\tau_1) + e^{2ik\tau_1} (i + k\tau_1)) c_s^4(\tau_1) v_{p_{ci}}(\tau_1) v_{p_{cj}}(\tau_1) \right|^2, \quad (34)$$

where the integral over  $\tau_1$  is performed in a numerical way. For the induced GWs generated in the inflationary epoch, the abundance of the relic GW energy spectrum at present can be approximated as [94]

$$\Omega_{\text{GW}}(\tau_0, k) h^2 \simeq 10^{-6} P_h^{\text{Inf}}(k, \tau \simeq 0). \quad (35)$$

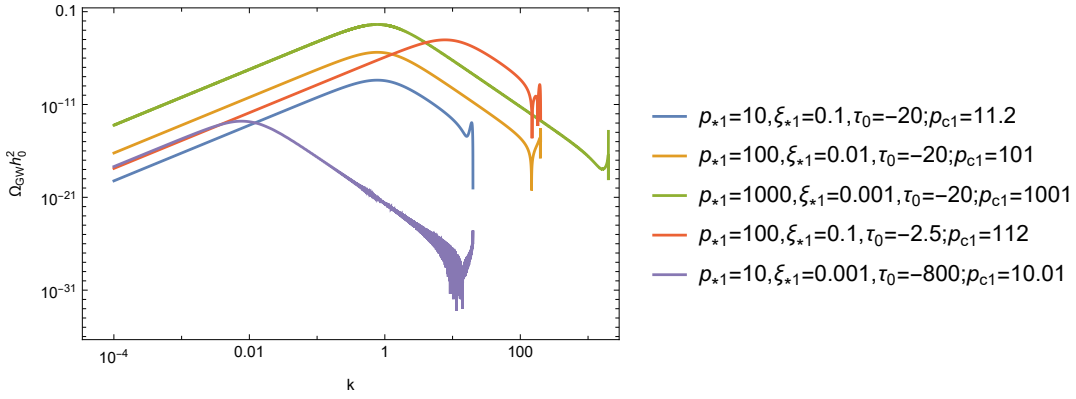


FIG. 4. The energy spectrum of induced GWs from inflationary era for single cosine  $c_s$  parameterization by setting  $\xi_{*2} = 0$ . Note that here we forget about the constraint  $P_h^{\text{Inf}} < 1$ , thus we are free to adjust the parameters. Similar to the upper-left panel in Fig.2, the source spectrum  $P_\zeta$  for each parameter set here contains only one dominant narrow peak  $p_{c1}$ , which is in the neighborhood of the characteristic scale  $p_{*1}$ . The spectrum curves show that the major broad peaks of GWs induced by certain  $p_{c1}$ -modes are located at  $\sim p_{c1}\xi_1$ .

Again,  $P_h^{\text{Inf}}(k, \tau \simeq 0)$  has to be smaller than unity, namely  $\Omega_{\text{GW}}(\tau_0, k)h^2 \lesssim 10^{-6}$ , to insure that all analysis is performed within perturbative regime. It is worth noting that in both Eqs.(28),(34), one can see that the convolution of resonating  $p_{ci}$ - and  $p_{cj}$ - modes ( $p_{ci}$  can equal to  $p_{cj}$ ) contributes to the overall GWs with wave-number  $k$  subjected to the window  $|p_{ci} - p_{cj}| < k < p_{ci} + p_{cj}$ . Moreover, just as the scale invariance of the scalar source spectrum, the GW power spectrum  $P_h$  as well as the energy density fraction  $\Omega_{\text{GW}}$  for both RD and inflationary cases, i.e. Eqs.(24), (27), (34) and (35), all remain invariant with the rescaling  $p_{ci} \rightarrow p_{ci}/\alpha, k \rightarrow k/\alpha, \tau \rightarrow \alpha\tau$  and  $v_p \rightarrow \sqrt{\alpha}v_p$ .

We first apply Eqs.(34),(35) to the case with single cosine parameterization of the sound speed, and display the induced GW energy spectrum for different parameters in Fig.4. For vanishing  $\xi_{*2}$ , only one narrow dominant  $p_{c1}$ -peak appears in source spectrum, and the corresponding resonating  $p_{c1}$ -mode leads to GW spectrum with a major peak at  $\sim p_{c1}\xi_1$ . In fact, this conclusion can be generalized to the case with multiple dominant peaks appearing in double cosine  $c_s$  scenario; the major broad peak of the each component of the GW spectrum induced by the corresponding resonating  $p_{ci}$ -mode is located at  $\sim p_{ci}\xi_i$ . This is evident in Fig.5, where we plot overall GW spectrum consisting of some components with the convolution of certain  $p_{ci}$ & $p_{cj}$ - modes (see Eq.(34)) in inflationary era for different parameter sets. Accordingly, for the same parameters as Fig.2, the positions of major peaks of all  $p_{ci}$ & $p_{cj}$  components are at  $\sim p_{ci}\xi_i \sim p_{*1}\xi_{*1} \sim p_{*2}\xi_{*2} \sim 1$ , leading to a single main peak in the overall GW spectrum. This marks a visible difference to the overall GW spectrum in RD era usually with two principle peak-like structure at  $\sim p_{*1}$  and  $\sim p_{*2}$  (see Fig.3). As mentioned in the RD case, here we also only need to take into account the dominant peaks, since the sub-dominant peaks contribute little to the overall GW energy density as illustrated in the lower-left panel in Fig.5. Next, let us focus on the first sharp significant spike on the right tail of the overall inflationary GW spectrum shown in Fig. 5. One can see that such spike receives the contributions only from the  $p_{ci}$ & $p_{ci}(i = 2, 3, \dots)$ -curves, not the  $p_{c1}$ & $p_{c1}$ - and  $p_{ci}$ & $p_{cj}(i \neq j, j = 1, 2, 3, \dots)$ -curves<sup>1</sup>. Let us note that  $p_{c1}$ & $p_{c1}$ -curves in the upper-left and lower-right panels do not have prominent spike at the same location of first sharp spike of the overall GW spectrum. Furthermore, one can see that the first sharp spikes of all  $p_{ci}$ & $p_{ci}(i = 2, 3, \dots)$ -curves share a common position at around  $k \simeq 20 \simeq 2p_{*1}$ . On the other hand, as displayed in Fig. 1, one remarkable difference among the  $p_{c1}$ -mode and  $p_{ci}(i = 2, 3, \dots)$ -modes is the presence of the small oscillations in the envelope of  $p_{ci}(i = 2, 3, \dots)$ -mode functions, whose oscillatory frequencies  $\omega_i$  share a common characteristic frequency  $\omega_i = p_{*1}$  (see Eq. (6)). Therefore, it is quite reasonable to relate these two common phenomena, and we interpret it as the fact that the oscillatory modulation of mode envelope generates a new resonance effect, related to the first sharp spike on inflationary GW spectrum. In order to investigate the role of the presence of the sinusoidal modulation of the envelope, in Fig.6 a comparison of the GW spectra, induced by the resonating modes with different magnitudes and frequencies in their envelope oscillations, is displayed. Indeed, one can see that the amplitude of the first narrow sharp spike in GW spectrum is proportional to the magnitude of envelope's oscillation; meanwhile the frequency  $\omega$  of the envelope oscillation primarily determines the position of the sharp peak located at  $\sim 2\omega$ . This is exactly our interpretation for the phenomena as in Fig. 5:  $p_{c1}$ & $p_{c1}$ -curve does not have such spike because  $p_{c1}$ -mode function does not have the envelope oscillation; the first

<sup>1</sup> Let us note that there is only one dominant resonating peak in the  $p_{*1}$ -peak group and normally more than one dominant resonating peak in  $p_{*2}$ -peak group (see Fig. 2). In order to clarify such a statement, here we denote  $p_{c1}$  the dominant resonating peak in the  $p_{*1}$ -peak group, and  $p_{ci}(i = 2, 3, \dots)$  dominant resonating peaks in the  $p_{*2}$ -peak group.

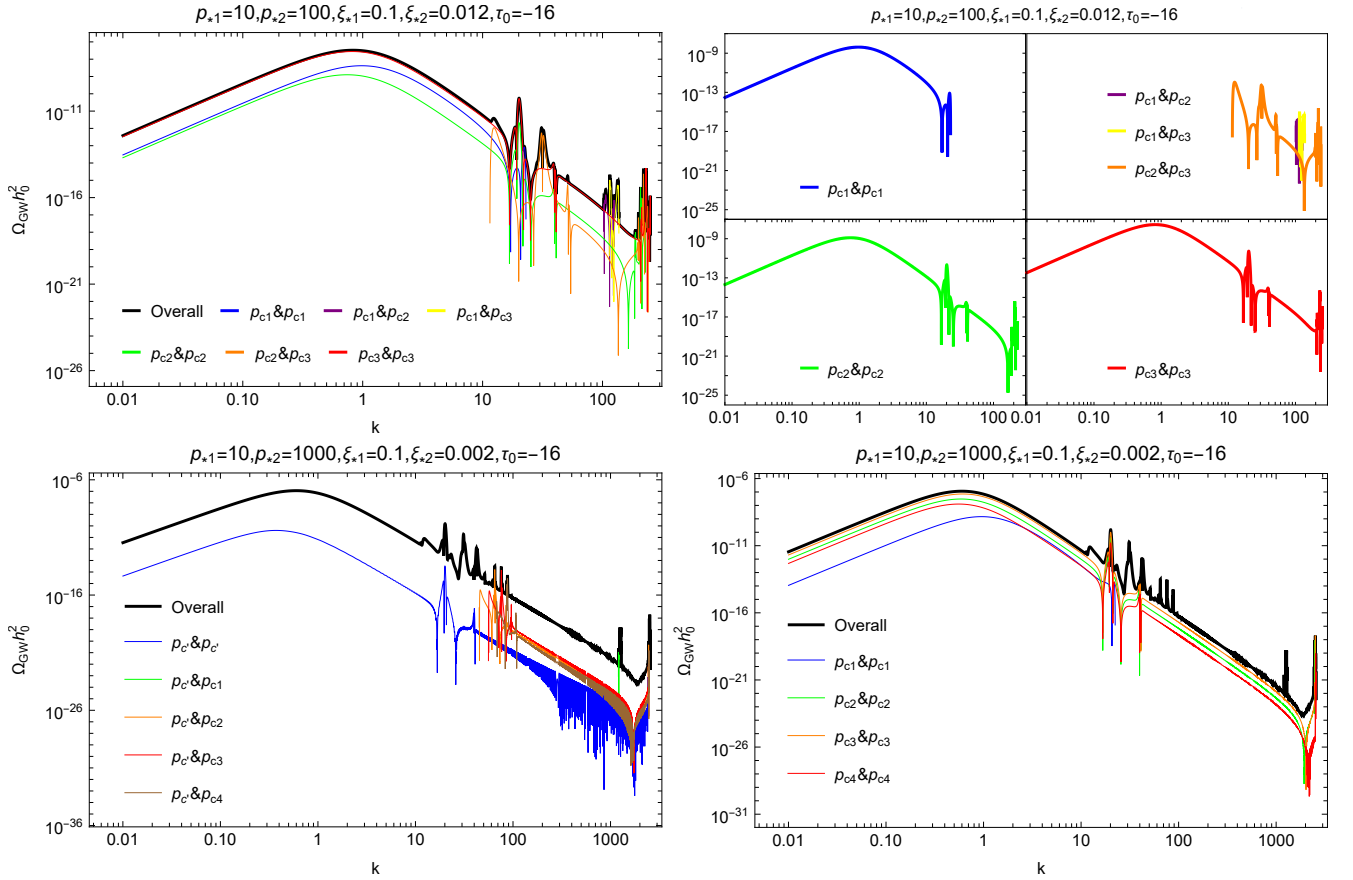


FIG. 5. The energy spectrum of induced GWs from inflationary era for parameter sets as those in lower panels in Fig. 2. The black line denotes the overall GW energy spectrum, which consists of the components generated by the convolution of dominant resonating  $p_{ci}$ - and  $p_{cj}$ -modes (see Eq.(34)). Note that each  $p_{ci}$ -mode corresponds to the narrow  $p_{ci}$ -peak in Fig. 2. As displayed in the lower-left panel, the components involved with the sub-dominant  $p_{c'}$ -mode (see the lower-right panel in Fig. 2) has irrelevant contributions to the overall GW spectrum, indicating that the main features of the GW spectrum are related to dominant  $p_{ci}$ -peaks. Contrary to the conventional two principle peak-like structures at  $\sim p_{*1}$  and  $\sim p_{*2}$  in the GW spectrum during RD era (see Fig. 3), in the inflationary GW spectrum there is only a single main broad peak at  $\sim p_{*1}\xi_{*1} \sim p_{*2}\xi_{*2} \sim 1$  since all  $p_{ci}\&p_{ci}$ -components have the major peaks at  $\sim p_{ci}\xi_i \sim 1$  for the given parameters. Moreover, it is interesting to observe that all  $p_{ci}\&p_{ci}$ -curves with  $p_{ci}$ -mode belonging to the  $p_{*2}$ -peak group share a common feature with a sharp spike at  $\sim 2p_{*1}$ , dominantly contributing to the first significant sharp peak in the intermediate band of the overall GW spectrum.

sharp spikes of all  $p_{ci}\&p_{ci}$  ( $i = 2, 3, \dots$ )-curves share a common position at around  $k \simeq 2\omega_i = 2p_{*1} = 20$ . The secondary peak in GW spectrum induced by the oscillatory modulation of the envelope of the resonating modes in  $p_{*2}$ -peak group can be viewed as a new kind of the resonance mechanism, which is unique from the double cosine parameterization of sound speed. Moreover, as in the RD case, the intersection effect of different  $p_{ci}$ - and  $p_{cj}$ - modes can produce multiple sharp spikes in the band range  $|p_{ci} - p_{cj}| < k < p_{ci} + p_{cj}$  of the overall GWs spectrum (see the upper-right panel in Fig. 5 for instance). On the other hand, it is worth to mention that irregular rapid oscillation for the GW spectrum with much lower magnitude  $\Omega_{GW} h_0^2 \lesssim 10^{-25}$  is interpreted as numerical noise, for instance, the blue line at  $k \gtrsim 200$  in the lower-left panel in Fig. 5, and the red line at  $f \gtrsim 1\text{Hz}$  in the lower-right panel in Fig. 7. In short, the typical profile of the inflationary GWs induced by the double sound speed resonances consists of a single broad peak at  $k \sim p_{*1}\xi_{*1} \sim p_{*2}\xi_{*2} \sim 1$ , followed by several significant multiple peaks on the right tail at  $k \sim 2p_{*1}$ , and possible irregular rapid oscillation in regime with much low magnitude  $\Omega_{GW} h_0^2 \lesssim 10^{-25}$ .

#### IV. PHENOMENOLOGICAL IMPLICATIONS

In this section, we will compare GW signals generated from inflationary and RD epochs with GW experiments [95], e.g., the Laser Interferometer Space Antenna (LISA) [96], DECI-hertz Interferometer Gravitational Wave Observatory

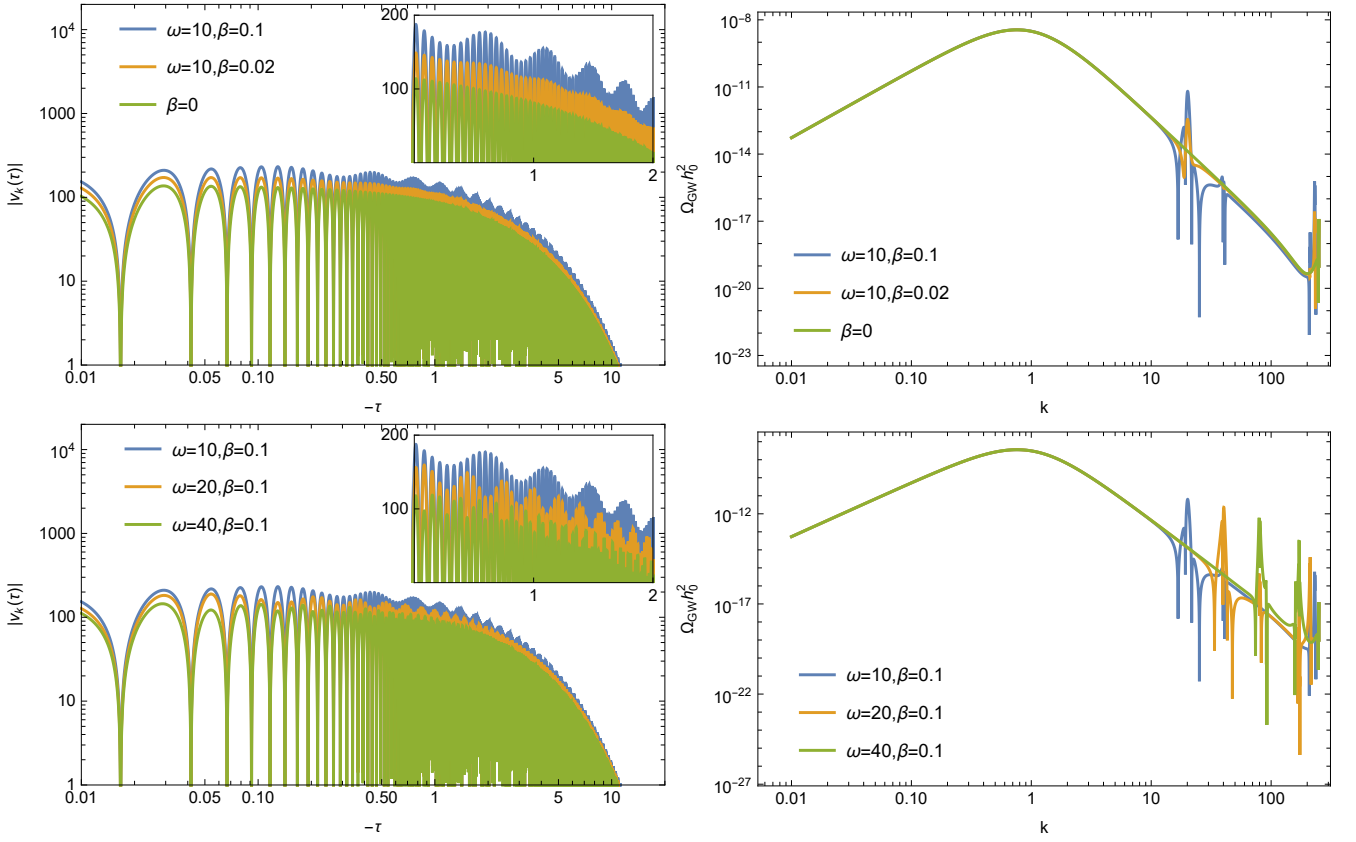


FIG. 6. The resonating modes with different magnitudes and frequencies in their envelope sinusoidal modulation (left column) and the corresponding induced GW spectra (right column). In the left column, the blue line represents a  $|v_p|$  solution of the  $p_{c3}$ -mode shown in Fig.1, whereas the other curves denote numerical solutions from Eq.(6), which are set as the control group with adjusted shapes of the envelopes. In the upper row, we find that amplitude of the first sharp spike in GW spectrum is proportional to the magnitude of the envelope oscillation, which disappears for vanishing  $\beta$  parameter. Moreover, as demonstrated in the lower row, the frequency  $\omega$  of the envelope oscillation shifts the position of the first sharp spike in GW spectrum as  $\sim 2\omega$ .

(DECIGO) [97, 98], BigBang Observer (BBO) [99, 100], Advanced LIGO + Virgo collaboration [101, 102], Einstein Telescope (ET) [103, 104] and Cosmic Explorer (CE) [105, 106]. For a clear comparison of theory with the sensitivity curves of GW observations, we use the GW frequency  $f^{GW}/\text{Hz}$  instead of the wave-number  $k/\text{Mpc}^{-1}$  by the relation  $f^{GW} = 1.55 \times 10^{-15} \left( \frac{k}{\text{Mpc}^{-1}} \right) \text{Hz}$ . For convenience, we introduce the frequency of the scalar source mode  $f^S/\text{Hz}$  related to its wave-number  $p/\text{Mpc}^{-1}$  by  $f^S = 1.55 \times 10^{-15} \left( \frac{p}{\text{Mpc}^{-1}} \right) \text{Hz}$ . Accordingly, we provide a dictionary among the characteristic scales  $p_{*1,2}$  and  $f_{*1,2}^S$ , the dominant resonating modes  $p_{ci}$  and  $f_{ci}^S$ , and so on. Let us notice that all previous results above can be easily regained in terms of  $f^{GW,S}$ . On the other hand, due to the scaling invariance of the GW energy spectrum mentioned below Eq.(35), we choose to fix one of the characteristic wave-number  $p_{*1}$  in double cosine  $c_s$  parameterization to be  $p_{*1} = 10^{13} \text{Mpc}^{-1}$ , i.e.  $f_{*1}^S \simeq 10^{-2} \text{Hz}$ , which falls in the optimal sensitivity window of LISA. Employing Eqs.(28), (34) and (35) for different ratios  $r \equiv f_{*2}^S/f_{*1}^S$ , we show a comparison among the induced GW abundance from inflationary and RD phases with the sensitivity curves of various GW observations in Figs.7 and 8. We mention that in all cases, the conditions are  $P_\zeta < 1$  and  $P_h < 1$ , or equivalently  $\Omega_{\text{GW}}(\tau_0, f)h_0^2 \lesssim 10^{-6}$ , avoiding the loss of the perturbative control for both the inflationary and RD eras.

In Fig.7, the parameters in the first three panels are simply rescaled of those in Fig.2, indicating that the profile of the corresponding source spectrum  $P_\zeta$  remains the same except a overall shift in the scale of  $p$  (or  $f^S$ ) due to scale invariance. More precisely, in the  $(P_\zeta, f^S)$  plane after rescaling, there exists one dominant resonating peak in the “ $f_{*1}^S$ -peak group” (similar definition as “ $p_{*1}$ -peak group” given in Sec. II) centered at  $\sim f_{*1}^S$ , and usually multiple dominant peaks in the “ $f_{*2}^S$ -peak group” centered at  $\sim f_{*2}^S$ . In Fig.7, one can see that the magnitude of the present GW energy spectrum from inflation era can be comparable to or even larger than that from the RD era. As discussed in Sec. III, the major broad peak of the GW spectrum from inflation is located at  $f^{GW} \sim f_{ci}^S \xi_i \sim f_{*1}^S \xi_{*1} \sim f_{*2}^S \xi_{*2} \sim 10^{-3} \text{Hz}$

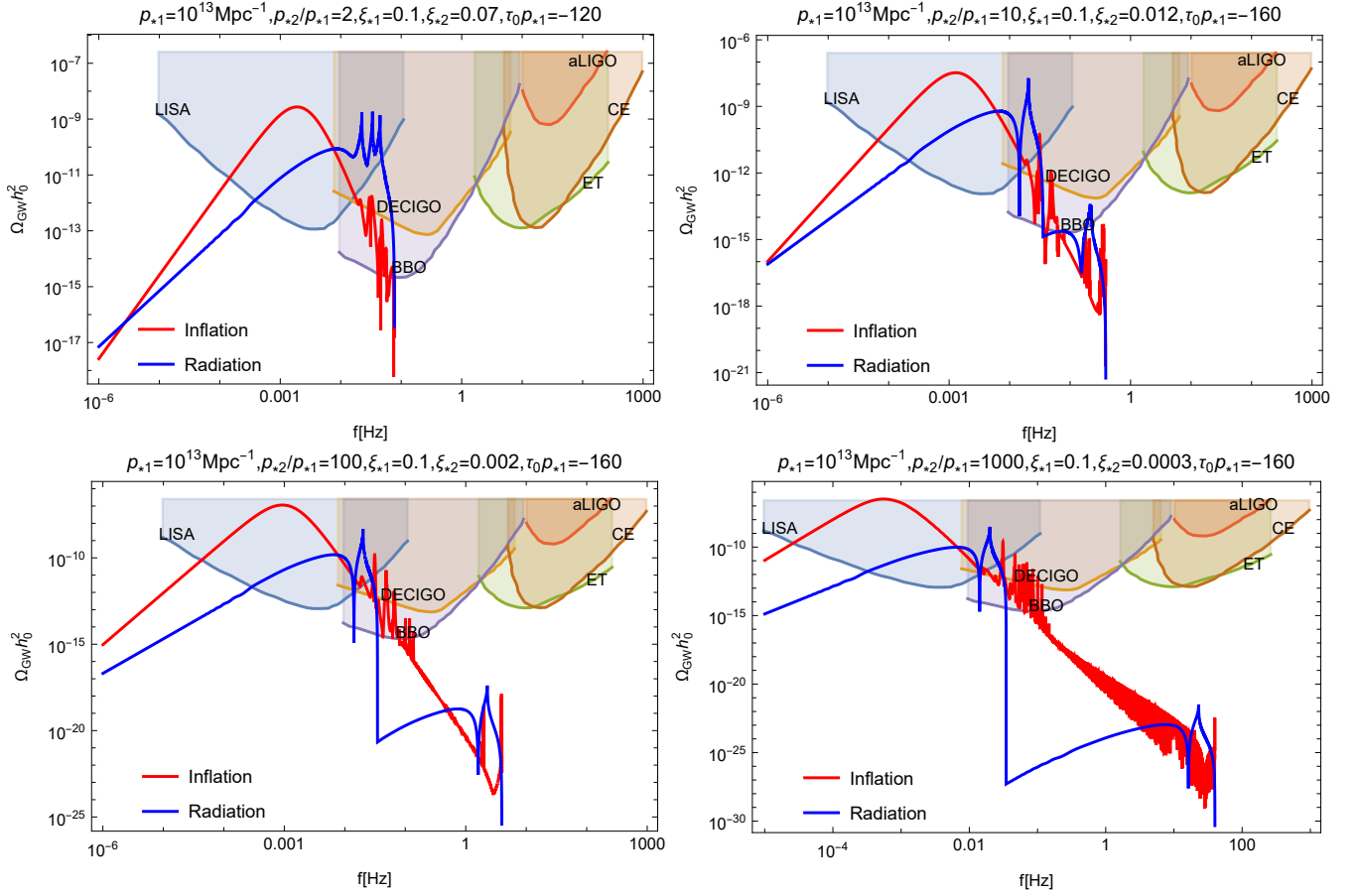


FIG. 7. A comparison between GW energy spectrum with sensitivity curves of LISA, DECIGO, BBO, aLIGO, ET and CE. By virtue of the scaling property, a fiducial scale is set to  $p_{*1} = 10^{13} \text{Mpc}^{-1}$  (i.e.  $f_{*1}^S \simeq 10^{-2} \text{Hz}$ ) corresponding to the optimal sensitivity window of LISA, and we plot the induced GW spectra from inflationary (red line) and RD eras (blue line) for different ratios  $r \equiv f_{*2}^S/f_{*1}^S = p_{*2}/p_{*1}$ . Notice that the parameters in  $r = 2, 10, 100$  cases are simply the rescaling of those in Fig. 2, which indicates that the profile of the GW spectrum shares the same features as the corresponding one in Fig. 3 and Fig. 5. The abundance of the relic GWs from inflationary era are comparable to that from the RD era. In all cases, the major peak of the inflationary GWs spectrum located at  $f^{GW} \sim f_{*1}^S \xi_{*1} \sim f_{*2}^S \xi_{*2} \sim 10^{-3} \text{Hz}$  overlaps with the sensitivity regime of LISA, and the multiple spikes in the intermediate band ( $10^{-2} \text{Hz}, 10^{-1} \text{Hz}$ ), originated from the effect of envelope oscillatory modulation and the intersection of multiple resonating source peaks, are in the sensitivity window of DECIGO/BBO. For the RD GW spectrum, a single principal peak-like structure at  $f^{GW} \sim f_{*1}^S$  for  $r = 2$ , whereas two principle peak-like structures at  $f^{GW} \sim f_{*1}^S$  and  $\sim f_{*2}^S$  for relatively large  $r$ . Such a principle peak-like configuration could possibly have localized fine features with multiple small spikes (see Fig. 3). The RD GW spectrum at  $\sim 10^{-2} \text{Hz}$  region can be probed by LISA/DECIGO/BBO for all cases here. For  $r = 10$  case, it lies into the BBO sensitivity limit at  $\sim 10^{-1} \text{Hz}$  region (upper-right panel), but it is far below the sensitivity of next future GW detectors for  $r = 100, 1000$  cases (lower panels).

in all cases shown in Fig. 7, which probes the sensitivity range of LISA. In the tail of the inflationary GW spectrum, multiple spikes fall within the sensitivity band of DECIGO/BBO in the ( $10^{-2} \text{Hz}, 10^{-1} \text{Hz}$ ) region, generated by the oscillatory modulation of the envelope (see Fig. 6) and the convolution of different resonating source modes (see Fig. 5). However, for the induced GW spectrum from RD era, its primary profile is sensitive to the positions and amplitudes of the dominant multiple peaks in source spectrum (see Figs. 2 and 3). In Fig. 7, GW spectrum exhibits only a principle peak-like structure at  $f^{GW} \sim f_{*1}^S \sim 10^{-2} \text{Hz}$  for small ratio  $r = 2$ , whereas two principle peak-like structures at  $f^{GW} \sim f_{*1}^S \sim 10^{-2} \text{Hz}$  and  $f^{GW} \sim f_{*2}^S \sim r \times 10^{-2} \text{Hz}$  for relatively large ratios  $r = 10, 100, 1000$ , respectively. On top of the principal peak-like structure, localized features with multiple small spikes can appear as shown in Fig. 3. We find that the RD GW spectrum at  $f^{GW} \sim f_{*1}^S \sim 10^{-2} \text{Hz}$  band lies in the sensitivity regime of LISA/DECIGO/BBO for all cases in Fig. 7 and at  $f^{GW} \sim f_{*2}^S \sim r \times 10^{-2} \text{Hz}$  band the BBO sensitivity limit for  $r = 10$  (upper-right panel); while far below the signal sensitivity available to the next generation of detector for  $r = 100, 1000$  (lower panels). In fact, to ensure the detectability of the RD GW peaks at LISA frequency window, the dimensionless combination  $p_{*1} \tau_0$  controlling the height of the dominant peak in the  $f_{*1}^S$ -peak group is set to be large enough for cases in Fig. 7.



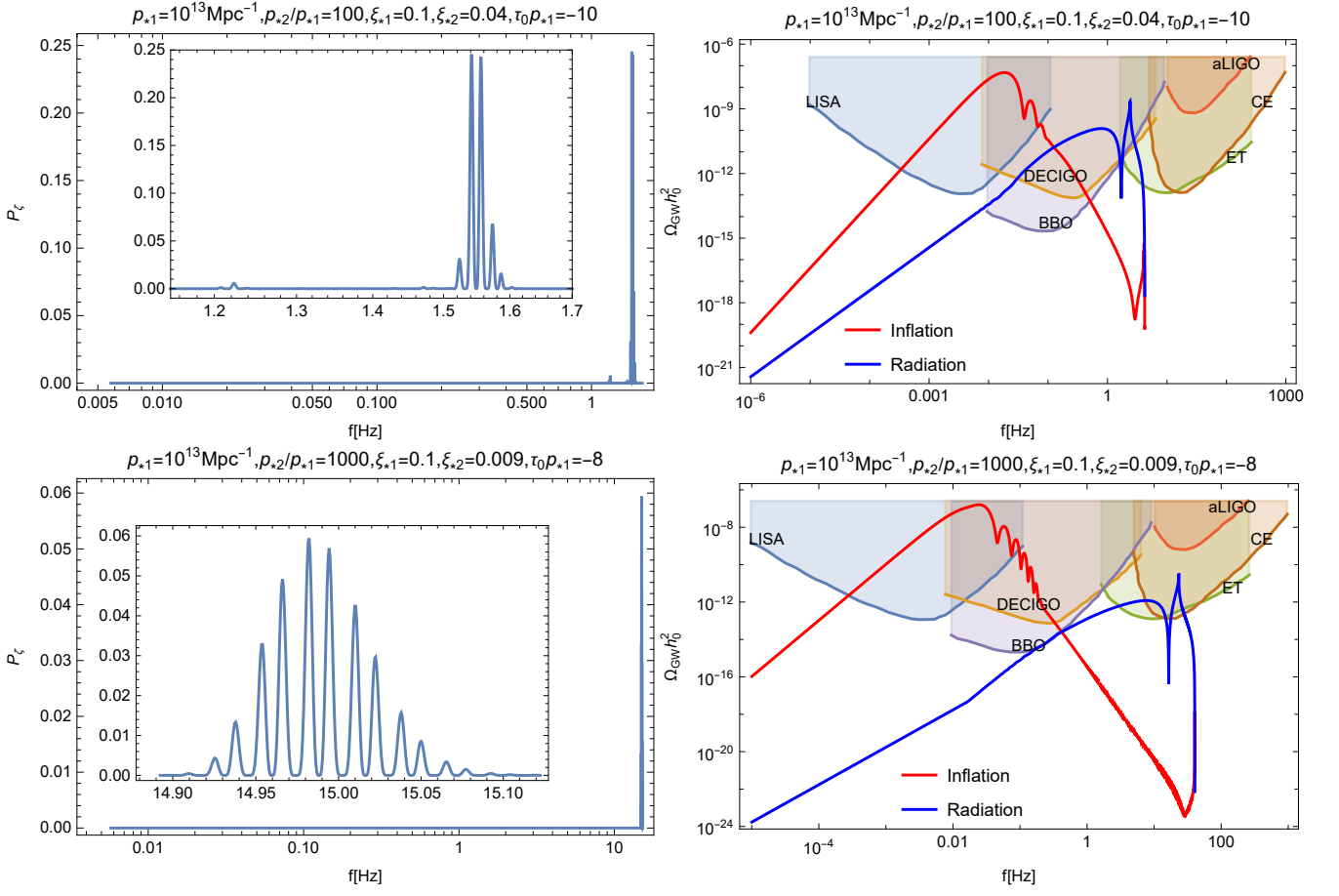


FIG. 8. The power spectrum of the primordial curvature perturbations, for relatively small value of dimensionless combination  $p_{*1}\tau_0$  (left column), and the corresponding GW energy spectrum compared with LISA, DECIGO, BBO, aLIGO, ET and CE (right column). We take the fiducial scale  $p_{*1} = 10^{13}\text{Mpc}^{-1}$ , i.e.  $f_{*1}^S \simeq 10^{-2}\text{Hz}$ , and display the cases with  $r = 100$  (upper row) and  $r = 1000$  (lower row). Differently to patterns shown in Fig.2 and Fig.7, one can see that the  $f_{*1}^S$ -peak group in the source spectrum as well as the peak-like structure in RD GW spectrum at  $f^{GW} \sim f_{*1}^S$  become invisible; meanwhile the  $\mathcal{O}(0.1)$  scale of dominant peaks in  $f_{*2}^S$ -peak group significantly amplify the RD GW spectrum at  $f^{GW} \sim f_{*2}^S$ . The resulted single peak RD GW spectrum now can be probed in the sensitivity region of DECIGO/BBO (ET/CE) at  $f^{GW} \sim f_{*2}^S \sim 1\text{Hz}(10\text{Hz})$  for  $r = 100(1000)$ . On the other hand, the major features of inflationary GW spectrum almost remain the same with only a tiny shift of overall scale (compare to Fig.7), namely the main broad peak is now shifted to  $f^{GW} \sim 0.01\text{Hz}$ , still visible for LISA.

Consequently,  $\xi_{*2}$  shall be small enough to meet the constraints  $P_c < 1$  and  $P_h < 1$ , which render the  $f_{*2}^S$ -peak group in source spectrum (the principle peak-like structure at  $f^{GW} \sim f_{*2}^S$  in RD GW spectrum) lower than the  $f_{*1}^S$ -peak group (the principle peak-like structure at  $f^{GW} \sim f_{*1}^S$  in RD GW spectrum) of around  $2 \sim 4$  ( $4 \sim 16$ ) orders of magnitude for large  $r$ . Therefore, in order to increase the magnitude of RD GW band at  $\sim f_{*2}^S$  for  $r = 100, 1000$ , the price to pay is to reduce the amplitude of the  $f_{*1}^S$ -peak group of source spectrum, and hence decreasing the RD GW abundance at  $f^{GW} \sim f_{*1}^S$ . Indeed, as displayed in Fig. 8, by taking much smaller  $p_{*1}\tau_0$ , the  $f_{*1}^S$ -peak group in source spectrum as well as the corresponding peak in RD GW spectrum become invisible, meanwhile the dominant peaks in  $f_{*2}^S$ -peak group increase to the  $\mathcal{O}(0.1)$  scale, leading to a significant amplification of RD GW abundance at  $f^{GW} \sim f_{*2}^S$  band. For  $r = 100$  the RD GW spectrum peak at  $f^{GW} \sim f_{*2}^S \sim 1\text{Hz}$  can be testable in DECIGO/BBO, and for  $r = 1000$  it is expected to be visible in the ET/CE band at  $f^{GW} \sim 10\text{Hz}$ . On the other hand, comparing Fig. 7 and Fig. 8, we find that the main features of inflationary GW spectrum are almost unchanged with only a slight overall shift and the major broad peak (now at  $\sim 0.01\text{Hz}$ ) is still visible for LISA. Let us notice that here the multiple spikes in the intermediate band of the inflationary GW spectrum have same origins as those in Fig. 7, namely from the intersection effect of the multiple resonating peaks and the parametric resonances of the envelope oscillatory modulation(see Fig. 9).

Furthermore, thanks to the scale invariance, both the overall GW spectra from RD and inflationary epochs can be shifted along the frequency axis by freely setting a fiducial frequency to  $f_{*1}^S$ . This implies that the induced GWs can



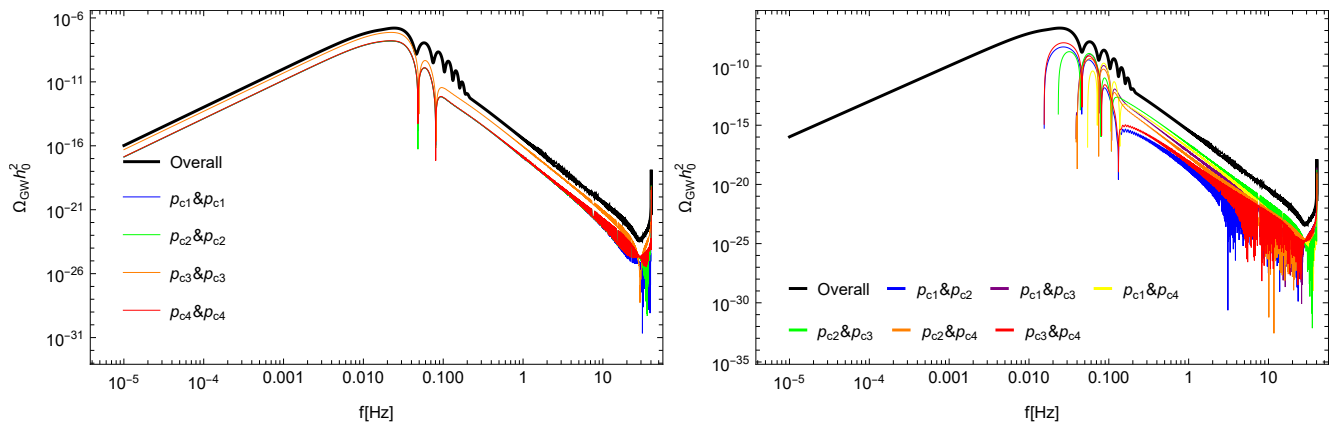


FIG. 9. The energy spectrum of induced GWs from inflationary era with parameter set as in lower panels in Fig. 8, namely  $p_{*1} = 10^{13} \text{Mpc}^{-1}$ ,  $p_{*2}/p_{*1} = 1000$ ,  $\xi_{*1} = 0.1$ ,  $\xi_{*2} = 0.009$ ,  $\tau_0 p_{*1} = -8$ . The black line denotes the overall GW energy spectrum, and the other colored lines denote the decomposed components (see Eq. (34)) generated by the convolution of several representative dominant resonating  $p_{ci}$ -modes displayed in the lower-left panel in Fig. 8. Similar to the analysis in Figs. 5 and 6, both the parametric resonances of envelope oscillatory modulation of each  $p_{ci}$ -mode (left panel) and intersection effect of the different  $p_{ci} \& p_{cj}$ -modes (right panel) make contributions to the oscillatory pattern in the intermediate band of the overall inflationary GWs spectrum. Moreover, the appearance of such regular GW oscillation (black line) is also sensitive to the particular oscillatory profile of multiple dominant resonating peaks in  $P_\zeta$  shown in the lower-left panel in Fig. 8.

overlap with each sensitivity range of all GW detectors. For instance, taking  $p_{*1} = 10^7 \text{Mpc}^{-1}$ , i.e.  $f_{*1}^S \simeq 10^{-8} \text{Hz}$ , some certain major peaks of RD and inflationary GW spectra can be at lower frequencies around  $f^{GW} \sim 10^{-8} \text{Hz}$  in the sensitive window accessible by the ongoing and planned pulsar timing array experiments such as the North American Nanohertz Observatory for Gravitational Waves (NANOGrav) [107, 108], Square Kilometre Array (SKA) [109] and International Pulsar Timing Array (IPTA) [110].

## V. DISCUSSION AND CONCLUSIONS

In this paper, we investigated the parametric resonance effects from the modified time-varying sound speed with the double oscillatory behavior. Sound speed resonances enhance the primordial density perturbations and hence amplify the abundance of the second order GWs induced during inflationary and RD epochs. We performed a comprehensive analysis from both theoretical and phenomenological sides. The resonant modes manifest themselves as narrow and sharp peaks in the power spectrum of the primordial density perturbations, amplifying the production of GWs during the inflationary and RD eras. GWs from early Universe dynamics survive as a characteristic stochastic background at the present day. We showed that a *resonance gravitational memory* of sound-speed oscillations during inflation is carried by the relic stochastic GW background and it can be detected by next generation of GW interferometers. The presence of two oscillatory modes in the sound speed yields interesting results. The two characteristic frequencies in Eq.(4) generically lead to multiple resonating peaks distributed in two groups centered around  $p_{*1}$  and  $p_{*2}$  in  $P_\zeta$  (see Figs.1 and 2), except some extreme cases like vanishing  $\beta_{*2}$  (see the upper-left panel in Fig.2) and very small value of  $p_{*1} \tau_0$  (see the left column in Fig.8). The appearance of multiple peaks, especially the dominant peak(s) in each group, characterize the spectrum of the induced GWs. Specifically, for the parameter space within the perturbative regime, there exists a single broad peak of the GW spectrum from inflation, the tails of which consist of multiple secondary spikes. The secondaries are generated by the convolution of multiple dominant peaks in source spectrum as well as the oscillatory modulation of certain resonating modes' envelope (see Figs.5-6). On the other hand, GW spectrum from RD epoch exhibits one (two) principle peak-like configuration at  $\sim p_{*1}$  ( $\sim p_{*1}$  and  $\sim p_{*2}$ ) for relatively small (large) ratio  $r = p_{*2}/p_{*1}$ , which, in certain parametric regions, can contain a fine structure of spikes from multiple peaks in source spectrum (see Fig.3). Finally, we studied phenomenological implications by fixing a particularly interesting benchmark frequency  $p_{*1} = 10^{13} \text{Mpc}^{-1}$ . We found that the major peak of the inflationary GW spectrum can be detected in LISA, meanwhile the principle peak-like structure of RD GW spectrum at  $\sim 10^{-2} \text{Hz}$  overlaps with the sensitivity window of LISA/DECIGO/BBO. The other principle peak-like structure at  $\sim r \times 10^{-2} \text{Hz}$  results as sub-dominated by at least 5 orders of magnitude (see Fig.7). Moreover, in the extreme cases with very small  $p_{*1} \tau_0$ , the abundance of RD GWs at  $\sim r \times 10^{-2} \text{Hz}$  band is largely boosted and can be detected in DECIGO/BBO or ET/CE (see Fig.8). In short, the distinctive behavior of the present relic GW spectrum generated during inflationary and RD

epochs can be analyzed as complementary features of signals at different frequency windows. Such a phenomena can be promisingly detected in several current and next future GW experiments.

As it is well known, PBHs can be formed when the primordial density perturbations of certain modes are dramatically amplified after re-entering into the Hubble horizon [111, 112]. Accordingly, the presence of multiple resonating peaks in the spectrum of curvature perturbations definitely increases the abundance of PBHs. The amplitudes and positions of these peaks determine the mass spectrum and fraction of PBHs, in turn constrained by several observations [113–115]. Therefore, searches for induced GWs and PBHs produced in our model from electromagnetic surveys and GW interferometers appear as promising in the era of multi-messenger astronomy. On the other hand, the overly enhancement of the primordial density perturbations at certain scale unavoidably induces non-Gaussianities of relic GWs at non-linear order [86, 116–118]. Thus, multiple resonating primordial source modes predicted in our model could imprint characteristic non-Gaussianities in the induced GW bispectrum. We think that such an effect deserves future investigations beyond the purposes of this work.

We also mentioned above that the double cosine parameterization of the sound speed could be extended to a more general scenario as Eq. (3) with  $N$  characteristic oscillation modes. From the resonance patterns of the single and double cosine scenarios, we can envisage that, generically, there will be up to  $N$  groups of resonating peaks centered at  $\sim p_{*1}, p_{*2}, \dots, p_{*N}$  in the power spectrum of primordial curvature perturbations. For the parameter space within perturbative regime, one plausible result is that a single major broad peak appears in the inflationary GW spectrum, whereas  $N$  principle peak-like structures in the RD GW spectrum. In addition, in Refs.[25, 26, 74] the authors showed that the primordial scalar power spectrum at small scales can be exponentially enhanced in the multi-field inflationary paradigm with a sharp pivot in the inflationary trajectory. Usually, inflaton field(s) undergoes to strong oscillations after a sudden turn aforementioned. Thus it would be an intriguing possibility to study a related sound speed resonance mechanism in multifield inflationary scenarios [61, 75]. Furthermore, the power spectrum of primordial curvature perturbations exhibits oscillations in several frequency intervals, for certain parameter choices (e.g., the insets in Fig.8). Such cases can be considered as related to the spectra with particular sharp features as ones displayed in Fig.9 in Ref.[26]. Indeed, the spectrum of GWs sourced during inflationary and RD era would inherit richer localized oscillatory features superposing on the principal peak-like structures, beyond the delta-peak approximation adopted in this paper (see Eqs.(7), (28) and (34)). Finally, in this work we have observed an interesting phenomena: the sinusoidal modulation of the resonating modes' envelope boosts the energy density of GWs at a narrow band (see Fig.6). This could be considered as another kind of parametric resonance effect that deserves future investigations.

**Acknowledgements.** We thank Peng Wang, Shengfeng Yan, Chao Chen and Guangzhou Guo for their helpful discussions and suggestions. Q.Y. Gan work is supported by the scholarship from China Scholarship Council (CSC) under the Grant CSC No. 202106240085. A.A. work is supported by the Talent Scientific Research Program of College of Physics, Sichuan University, Grant No.1082204112427 & the Fostering Program in Disciplines Possessing Novel Features for Natural Science of Sichuan University, Grant No. 2020SCUNL209 & 1000 Talent program of Sichuan province 2021. S.C. acknowledges the support of Istituto Nazionale di Fisica Nucleare sez. di Napoli (*iniziativa specifica* QGSKY and Moonlight2).

- 
- [1] B. P. Abbott et al. Observation of Gravitational Waves from a Binary Black Hole Merger. *Phys. Rev. Lett.*, 116(6):061102, 2016. [arXiv:1602.03837](#), [doi:10.1103/PhysRevLett.116.061102](#). I
  - [2] B. P. Abbott et al. GW170817: Observation of Gravitational Waves from a Binary Neutron Star Inspiral. *Phys. Rev. Lett.*, 119(16):161101, 2017. [arXiv:1710.05832](#), [doi:10.1103/PhysRevLett.119.161101](#). I
  - [3] Guillem Domènech. Scalar Induced Gravitational Waves Review. *Universe*, 7(11):398, 2021. [arXiv:2109.01398](#), [doi:10.3390/universe7110398](#). I
  - [4] Viviana Acquaviva, Nicola Bartolo, Sabino Matarrese, and Antonio Riotto. Second order cosmological perturbations from inflation. *Nucl. Phys. B*, 667:119–148, 2003. [arXiv:astro-ph/0209156](#), [doi:10.1016/S0550-3213\(03\)00550-9](#). I, III A
  - [5] Daniel Baumann. Inflation. In *Theoretical Advanced Study Institute in Elementary Particle Physics: Physics of the Large and the Small*, pages 523–686, 2011. [arXiv:0907.5424](#), [doi:10.1142/9789814327183\\_0010](#). I
  - [6] Matteo Biagetti, Matteo Fasiello, and Antonio Riotto. Enhancing Inflationary Tensor Modes through Spectator Fields. *Phys. Rev. D*, 88:103518, 2013. [arXiv:1305.7241](#), [doi:10.1103/PhysRevD.88.103518](#). I, III B, III B
  - [7] Yi-Fu Cai, Chao Chen, Xi Tong, Dong-Gang Wang, and Sheng-Feng Yan. When Primordial Black Holes from Sound Speed Resonance Meet a Stochastic Background of Gravitational Waves. *Phys. Rev. D*, 100(4):043518, 2019. [arXiv:1902.08187](#), [doi:10.1103/PhysRevD.100.043518](#). I, II, II, II, III A, III A, III B, III B

- [8] Jacopo Fumagalli, Gonzalo A. Palma, Sébastien Renaux-Petel, Spyros Sypsas, Lukas T. Witkowski, and Cristobal Zenteno. Primordial gravitational waves from excited states. 11 2021. [arXiv:2111.14664](#). I, III B
- [9] Zhi-Zhang Peng, Chengjie Fu, Jing Liu, Zong-Kuan Guo, and Rong-Gen Cai. Gravitational waves from resonant amplification of curvature perturbations during inflation. *JCAP*, 10:050, 2021. [arXiv:2106.11816](#), [doi:10.1088/1475-7516/2021/10/050](#). I
- [10] Rong-Gen Cai, Chao Chen, and Chengjie Fu. Primordial black holes and stochastic gravitational wave background from inflation with a noncanonical spectator field. *Phys. Rev. D*, 104(8):083537, 2021. [arXiv:2108.03422](#), [doi:10.1103/PhysRevD.104.083537](#). I, III B
- [11] Keisuke Inomata. Bound on induced gravitational waves during inflation era. *Phys. Rev. D*, 104(12):123525, 2021. [arXiv:2109.06192](#), [doi:10.1103/PhysRevD.104.123525](#). I
- [12] Kishore N. Ananda, Chris Clarkson, and David Wands. The Cosmological gravitational wave background from primordial density perturbations. *Phys. Rev. D*, 75:123518, 2007. [arXiv:gr-qc/0612013](#), [doi:10.1103/PhysRevD.75.123518](#). I, III A, III A, III A
- [13] Daniel Baumann, Paul J. Steinhardt, Keitaro Takahashi, and Kiyotomo Ichiki. Gravitational Wave Spectrum Induced by Primordial Scalar Perturbations. *Phys. Rev. D*, 76:084019, 2007. [arXiv:hep-th/0703290](#), [doi:10.1103/PhysRevD.76.084019](#). III A, III A
- [14] Hooshyar Assadullahi and David Wands. Gravitational waves from an early matter era. *Phys. Rev. D*, 79:083511, 2009. [arXiv:0901.0989](#), [doi:10.1103/PhysRevD.79.083511](#).
- [15] Kazunori Kohri and Takahiro Terada. Semianalytic calculation of gravitational wave spectrum nonlinearly induced from primordial curvature perturbations. *Phys. Rev. D*, 97(12):123532, 2018. [arXiv:1804.08577](#), [doi:10.1103/PhysRevD.97.123532](#). I, III A
- [16] Pavel Ivanov, Pavel Naselsky, and Igor Novikov. Inflation and primordial black holes as dark matter. *Physical Review D*, 50(12):7173, 1994. I
- [17] Haoran Di and Yungui Gong. Primordial black holes and second order gravitational waves from ultra-slow-roll inflation. *JCAP*, 07:007, 2018. [arXiv:1707.09578](#), [doi:10.1088/1475-7516/2018/07/007](#).
- [18] Guillermo Ballesteros and Marco Taoso. Primordial black hole dark matter from single field inflation. *Phys. Rev. D*, 97(2):023501, 2018. [arXiv:1709.05565](#), [doi:10.1103/PhysRevD.97.023501](#).
- [19] Rafid Mahbub. Primordial black hole formation in inflationary  $\alpha$ -attractor models. *Phys. Rev. D*, 101(2):023533, 2020. [arXiv:1910.10602](#), [doi:10.1103/PhysRevD.101.023533](#).
- [20] H. V. Ragavendra, Pankaj Saha, L. Sriramkumar, and Joseph Silk. Primordial black holes and secondary gravitational waves from ultraslow roll and punctuated inflation. *Phys. Rev. D*, 103(8):083510, 2021. [arXiv:2008.12202](#), [doi:10.1103/PhysRevD.103.083510](#). I
- [21] K. Kefala, G. P. Kodaxis, I. D. Stamou, and N. Tetradis. Features of the inflaton potential and the power spectrum of cosmological perturbations. *Phys. Rev. D*, 104(2):023506, 2021. [arXiv:2010.12483](#), [doi:10.1103/PhysRevD.104.023506](#). I
- [22] Keisuke Inomata, Evan McDonough, and Wayne Hu. Amplification of Primordial Perturbations from the Rise or Fall of the Inflaton. 10 2021. [arXiv:2110.14641](#).
- [23] I. Dalianis, G. P. Kodaxis, I. D. Stamou, N. Tetradis, and A. Tsigkas-Kouvelis. Spectrum oscillations from features in the potential of single-field inflation. *Phys. Rev. D*, 104(10):103510, 2021. [arXiv:2106.02467](#), [doi:10.1103/PhysRevD.104.103510](#). I
- [24] Rong-Gen Cai, Zong-Kuan Guo, Jing Liu, Lang Liu, and Xing-Yu Yang. Primordial black holes and gravitational waves from parametric amplification of curvature perturbations. *JCAP*, 06:013, 2020. [arXiv:1912.10437](#), [doi:10.1088/1475-7516/2020/06/013](#). I, II
- [25] Gonzalo A. Palma, Spyros Sypsas, and Cristobal Zenteno. Seeding primordial black holes in multifield inflation. *Phys. Rev. Lett.*, 125(12):121301, 2020. [arXiv:2004.06106](#), [doi:10.1103/PhysRevLett.125.121301](#). I, V
- [26] Jacopo Fumagalli, Sébastien Renaux-Petel, and Lukas T. Witkowski. Oscillations in the stochastic gravitational wave background from sharp features and particle production during inflation. *JCAP*, 08:030, 2021. [arXiv:2012.02761](#), [doi:10.1088/1475-7516/2021/08/030](#). I, III A, V
- [27] Kristjan Kannike, Luca Marzola, Martti Raidal, and Hardi Veermäe. Single Field Double Inflation and Primordial Black Holes. *JCAP*, 09:020, 2017. [arXiv:1705.06225](#), [doi:10.1088/1475-7516/2017/09/020](#). I
- [28] Shi Pi, Ying-li Zhang, Qing-Guo Huang, and Misao Sasaki. Scalon from  $R^2$ -gravity as a heavy field. *JCAP*, 05:042, 2018. [arXiv:1712.09896](#), [doi:10.1088/1475-7516/2018/05/042](#).
- [29] Salvatore Capozziello, Mariafelicia De Laurentis, Shin'ichi Nojiri, and Sergei D. Odintsov. Evolution of gravitons in accelerating cosmologies: The case of extended gravity. *Phys. Rev. D*, 95(8):083524, 2017. [arXiv:1702.05517](#), [doi:10.1103/PhysRevD.95.083524](#).
- [30] Salvatore Capozziello and Francesco Bajardi. Gravitational waves in modified gravity. *Int. J. Mod. Phys. D*, 28(05):1942002, 2019. [doi:10.1142/S0218271819420021](#).
- [31] Chengjie Fu, Puxun Wu, and Hongwei Yu. Primordial Black Holes from Inflation with Nonminimal Derivative Coupling. *Phys. Rev. D*, 100(6):063532, 2019. [arXiv:1907.05042](#), [doi:10.1103/PhysRevD.100.063532](#).
- [32] Amjad Ashoorioon, Abasalt Rostami, and Javad T. Firouzjaee. EFT compatible PBHs: effective spawning of the seeds for primordial black holes during inflation. *JHEP*, 07:087, 2021. [arXiv:1912.13326](#), [doi:10.1007/JHEP07\(2021\)087](#).
- [33] Amjad Ashoorioon, Roberto Casadio, Michele Cicoli, Ghazal Geshnizjani, and Hyung J. Kim. Extended Effective Field Theory of Inflation. *JHEP*, 02:172, 2018. [arXiv:1802.03040](#), [doi:10.1007/JHEP02\(2018\)172](#).
- [34] Jiong Lin, Qing Gao, Yungui Gong, Yizhou Lu, Chao Zhang, and Fengge Zhang. Primordial black holes and secondary

- gravitational waves from  $k$  and  $G$  inflation. *Phys. Rev. D*, 101(10):103515, 2020. [arXiv:2001.05909](#), [doi:10.1103/PhysRevD.101.103515](#).
- [35] Shinsuke Kawai and Jinsu Kim. Primordial black holes from Gauss-Bonnet-corrected single field inflation. *Phys. Rev. D*, 104(8):083545, 2021. [arXiv:2108.01340](#), [doi:10.1103/PhysRevD.104.083545](#). I
- [36] Kenta Ando, Keisuke Inomata, Masahiro Kawasaki, Kyohei Mukaida, and Tsutomu T. Yanagida. Primordial black holes for the LIGO events in the axionlike curvaton model. *Phys. Rev. D*, 97(12):123512, 2018. [arXiv:1711.08956](#), [doi:10.1103/PhysRevD.97.123512](#). I
- [37] Keisuke Inomata, Masahiro Kawasaki, Kyohei Mukaida, and Tsutomu T. Yanagida. NANOGrav Results and LIGO-Virgo Primordial Black Holes in Axionlike Curvaton Models. *Phys. Rev. Lett.*, 126(13):131301, 2021. [arXiv:2011.01270](#), [doi:10.1103/PhysRevLett.126.131301](#).
- [38] Zihan Zhou, Jie Jiang, Yi-Fu Cai, Misao Sasaki, and Shi Pi. Primordial black holes and gravitational waves from resonant amplification during inflation. *Phys. Rev. D*, 102(10):103527, 2020. [arXiv:2010.03537](#), [doi:10.1103/PhysRevD.102.103527](#).
- [39] Shi Pi and Misao Sasaki. Primordial Black Hole Formation in Non-Minimal Curvaton Scenario. 12 2021. [arXiv:2112.12680](#).
- [40] Keisuke Inomata. Traces of a Heavy Field in Gravitational Waves. 3 2022. [arXiv:2203.04974](#). I
- [41] Mohsen Khodadi, Ujjal Kumar Dey, and Gaetano Lambiase. Strongly magnetized hot QCD matter and stochastic gravitational wave background. *Phys. Rev. D*, 104(6):063039, 2021. [arXiv:2108.09320](#), [doi:10.1103/PhysRevD.104.063039](#). I
- [42] Mohsen Khodadi, Kourosh Nozari, Habib Abedi, and Salvatore Capozziello. Planck scale effects on the stochastic gravitational wave background generated from cosmological hadronization transition: A qualitative study. *Phys. Lett. B*, 783:326–333, 2018. [arXiv:1805.11310](#), [doi:10.1016/j.physletb.2018.07.010](#).
- [43] Andrea Addazi, Yi-Fu Cai, Qingyu Gan, Antonino Marciano, and Kaiqiang Zeng. NANOGrav results and dark first order phase transitions. *Sci. China Phys. Mech. Astron.*, 64(9):290411, 2021. [arXiv:2009.10327](#), [doi:10.1007/s11433-021-1724-6](#). I
- [44] Ogan Özsoy and Zygunt Lalak. Primordial black holes as dark matter and gravitational waves from bumpy axion inflation. *JCAP*, 01:040, 2021. [arXiv:2008.07549](#), [doi:10.1088/1475-7516/2021/01/040](#). I
- [45] Yermek Aldabergenov, Andrea Addazi, and Sergei V. Ketov. Primordial black holes from modified supergravity. *Eur. Phys. J. C*, 80(10):917, 2020. [arXiv:2006.16641](#), [doi:10.1140/epjc/s10052-020-08506-6](#).
- [46] Lina Wu, Yungui Gong, and Tianjun Li. Primordial black holes and secondary gravitational waves from string inspired general no-scale supergravity. *Phys. Rev. D*, 104(12):123544, 2021. [arXiv:2105.07694](#), [doi:10.1103/PhysRevD.104.123544](#).
- [47] Fengge Zhang. Primordial black holes and scalar induced gravitational waves from E-model with Gauss-Bonnet term. 12 2021. [arXiv:2112.10516](#).
- [48] Vassilis C. Spanos and Ioanna D. Stamou. Gravitational waves and primordial black holes from supersymmetric hybrid inflation. *Phys. Rev. D*, 104(12):123537, 2021. [arXiv:2108.05671](#), [doi:10.1103/PhysRevD.104.123537](#).
- [49] Sergei V. Ketov. Multi-Field versus Single-Field in the Supergravity Models of Inflation and Primordial Black Holes. *Universe*, 7(5):115, 2021. [doi:10.3390/universe7050115](#). I
- [50] C. Armendariz-Picon, T. Damour, and Viatcheslav F. Mukhanov.  $k$  - inflation. *Phys. Lett. B*, 458:209–218, 1999. [arXiv:hep-th/9904075](#), [doi:10.1016/S0370-2693\(99\)00603-6](#). I
- [51] Jaume Garriga and Viatcheslav F. Mukhanov. Perturbations in  $k$ -inflation. *Phys. Lett. B*, 458:219–225, 1999. [arXiv:hep-th/9904176](#), [doi:10.1016/S0370-2693\(99\)00602-4](#). I
- [52] Eva Silverstein and David Tong. Scalar speed limits and cosmology: Acceleration from D-cceleration. *Phys. Rev. D*, 70:103505, 2004. [arXiv:hep-th/0310221](#), [doi:10.1103/PhysRevD.70.103505](#). I
- [53] Mohsen Alishahiha, Eva Silverstein, and David Tong. DBI in the sky. *Phys. Rev. D*, 70:123505, 2004. [arXiv:hep-th/0404084](#), [doi:10.1103/PhysRevD.70.123505](#). I
- [54] Ana Achucarro, Jinn-Ouk Gong, Sjoerd Hardeman, Gonzalo A. Palma, and Subodh P. Patil. Features of heavy physics in the CMB power spectrum. *JCAP*, 01:030, 2011. [arXiv:1010.3693](#), [doi:10.1088/1475-7516/2011/01/030](#). I
- [55] Ana Achucarro, Jinn-Ouk Gong, Sjoerd Hardeman, Gonzalo A. Palma, and Subodh P. Patil. Mass hierarchies and non-decoupling in multi-scalar field dynamics. *Phys. Rev. D*, 84:043502, 2011. [arXiv:1005.3848](#), [doi:10.1103/PhysRevD.84.043502](#). I
- [56] Hao Wei, Rong-Gen Cai, and Anzhong Wang. Second-order corrections to the power spectrum in the slow-roll expansion with a time-dependent sound speed. *Phys. Lett. B*, 603:95–106, 2004. [arXiv:hep-th/0409130](#), [doi:10.1016/j.physletb.2004.10.034](#).
- [57] Rachel Bean, Xingang Chen, Girma Hailu, S. H. Henry Tye, and Jiajun Xu. Duality Cascade in Brane Inflation. *JCAP*, 03:026, 2008. [arXiv:0802.0491](#), [doi:10.1088/1475-7516/2008/03/026](#).
- [58] Andrew J. Tolley and Mark Wyman. The Gelaton Scenario: Equilateral non-Gaussianity from multi-field dynamics. *Phys. Rev. D*, 81:043502, 2010. [arXiv:0910.1853](#), [doi:10.1103/PhysRevD.81.043502](#).
- [59] Masahiro Nakashima, Ryo Saito, Yu-ichi Takamizu, and Jun'ichi Yokoyama. The effect of varying sound velocity on primordial curvature perturbations. *Progress of theoretical physics*, 125(5):1035–1052, 2011.
- [60] Minjoon Park and Lorenzo Sorbo. Sudden variations in the speed of sound during inflation: features in the power spectrum and bispectrum. *Phys. Rev. D*, 85:083520, 2012. [arXiv:1201.2903](#), [doi:10.1103/PhysRevD.85.083520](#).
- [61] Xian Gao, David Langlois, and Shuntaro Mizuno. Oscillatory features in the curvature power spectrum after a sudden turn of the inflationary trajectory. *JCAP*, 10:023, 2013. [arXiv:1306.5680](#), [doi:10.1088/1475-7516/2013/10/023](#). I, V



- [62] Ana Achúcarro, Vicente Atal, Bin Hu, Pablo Ortiz, and Jesus Torrado. Inflation with moderately sharp features in the speed of sound: Generalized slow roll and in-in formalism for power spectrum and bispectrum. *Phys. Rev. D*, 90(2):023511, 2014. [arXiv:1404.7522](#), [doi:10.1103/PhysRevD.90.023511](#).
- [63] Sander Mooij, Gonzalo A. Palma, Grigoris Panotopoulos, and Alex Soto. Consistency relations for sharp features in the primordial spectra. *JCAP*, 10:062, 2015. [Erratum: *JCAP* 02, E01 (2016)]. [arXiv:1507.08481](#), [doi:10.1088/1475-7516/2015/10/062](#).
- [64] Carsten van de Bruck, Tomi Koivisto, and Chris Longden. Disformally coupled inflation. *JCAP*, 03:006, 2016. [arXiv:1510.01650](#), [doi:10.1088/1475-7516/2016/03/006](#).
- [65] Yong Cai, Yu-Tong Wang, and Yun-Song Piao. Oscillating modulation to B-mode polarization from varying propagating speed of primordial gravitational waves. *Phys. Rev. D*, 91:103001, 2015. [arXiv:1501.06345](#), [doi:10.1103/PhysRevD.91.103001](#).
- [66] Gonzalo A. Palma, Domenico Sapone, and Spyros Sypsas. Constraints on inflation with LSS surveys: features in the primordial power spectrum. *JCAP*, 06:004, 2018. [arXiv:1710.02570](#), [doi:10.1088/1475-7516/2018/06/004](#).
- [67] Guadalupe Cañas Herrera, Jesús Torrado, and Ana Achúcarro. Bayesian reconstruction of the inflaton’s speed of sound using CMB data. *Phys. Rev. D*, 103:123531, 2021. [arXiv:2012.04640](#), [doi:10.1103/PhysRevD.103.123531](#).
- [68] Guillermo Ballesteros, Sebastián Céspedes, and Luca Santoni. Large power spectrum and primordial black holes in the effective theory of inflation. *JHEP*, 01:074, 2022. [arXiv:2109.00567](#), [doi:10.1007/JHEP01\(2022\)074](#).
- [69] Salvatore Capozziello, Mohsen Khodadi, and Gaetano Lambiase. The quark chemical potential of QCD phase transition and the stochastic background of gravitational waves. *Phys. Lett. B*, 789:626–633, 2019. [arXiv:1808.06188](#), [doi:10.1016/j.physletb.2019.01.004](#). I
- [70] Yi-Fu Cai, Xi Tong, Dong-Gang Wang, and Sheng-Feng Yan. Primordial Black Holes from Sound Speed Resonance during Inflation. *Phys. Rev. Lett.*, 121(8):081306, 2018. [arXiv:1805.03639](#), [doi:10.1103/PhysRevLett.121.081306](#). I, II, II, II, II, II
- [71] Chao Chen, Xiao-Han Ma, and Yi-Fu Cai. Dirac-Born-Infeld realization of sound speed resonance mechanism for primordial black holes. *Phys. Rev. D*, 102(6):063526, 2020. [arXiv:2003.03821](#), [doi:10.1103/PhysRevD.102.063526](#).
- [72] Chao Chen and Yi-Fu Cai. Primordial black holes from sound speed resonance in the inflaton-curvaton mixed scenario. *JCAP*, 10:068, 2019. [arXiv:1908.03942](#), [doi:10.1088/1475-7516/2019/10/068](#). I
- [73] Yi-Fu Cai, Chunshan Lin, Bo Wang, and Sheng-Feng Yan. Sound speed resonance of the stochastic gravitational wave background. *Phys. Rev. Lett.*, 126(7):071303, 2021. [arXiv:2009.09833](#), [doi:10.1103/PhysRevLett.126.071303](#). I
- [74] Jacopo Fumagalli, Sébastien Renaux-Petel, John W. Ronayne, and Lukas T. Witkowski. Turning in the landscape: a new mechanism for generating Primordial Black Holes. 4 2020. [arXiv:2004.08369](#). I, V
- [75] Xingang Chen. Primordial Features as Evidence for Inflation. *JCAP*, 01:038, 2012. [arXiv:1104.1323](#), [doi:10.1088/1475-7516/2012/01/038](#). I, V
- [76] Jing Liu, Zong-Kuan Guo, Rong-Gen Cai, and Gary Shiu. Gravitational Waves from Oscillons with Cuspy Potentials. *Phys. Rev. Lett.*, 120(3):031301, 2018. [arXiv:1707.09841](#), [doi:10.1103/PhysRevLett.120.031301](#). I
- [77] Jing Liu, Zong-Kuan Guo, Rong-Gen Cai, and Gary Shiu. Gravitational wave production after inflation with cuspy potentials. *Phys. Rev. D*, 99(10):103506, 2019. [arXiv:1812.09235](#), [doi:10.1103/PhysRevD.99.103506](#).
- [78] Fengge Zhang, Jiong Lin, and Yizhou Lu. Double-peaked inflation model: Scalar induced gravitational waves and primordial-black-hole suppression from primordial non-Gaussianity. *Phys. Rev. D*, 104(6):063515, 2021. [arXiv:2106.10792](#), [doi:10.1103/PhysRevD.104.063515](#).
- [79] Qing Wang, Yi-Chen Liu, Bing-Yu Su, and Nan Li. Primordial black holes from the perturbations in the inflaton potential in peak theory. *Phys. Rev. D*, 104(8):083546, 2021. [arXiv:2111.10028](#), [doi:10.1103/PhysRevD.104.083546](#).
- [80] Tie-Jun Gao and Xiu-Yi Yang. Double peaks of gravitational wave spectrum induced from inflection point inflation. *Eur. Phys. J. C*, 81(6):494, 2021. [arXiv:2101.07616](#), [doi:10.1140/epjc/s10052-021-09269-4](#).
- [81] Ruifeng Zheng, Jiaming Shi, and Taotao Qiu. On Primordial Black Holes generated from inflation with solo/multi-bumpy potential. 6 2021. [arXiv:2106.04303](#). I
- [82] Ryo Saito and Jun’ichi Yokoyama. Gravitational-wave constraints on the abundance of primordial black holes. *Progress of theoretical physics*, 123(5):867–886, 2010. III A
- [83] José Ramón Espinosa, Davide Racco, and Antonio Riotto. A Cosmological Signature of the SM Higgs Instability: Gravitational Waves. *JCAP*, 09:012, 2018. [arXiv:1804.07732](#), [doi:10.1088/1475-7516/2018/09/012](#). III A, III A, III A, III A, III A
- [84] David H. Lyth and Antonio Riotto. Particle physics models of inflation and the cosmological density perturbation. *Phys. Rept.*, 314:1–146, 1999. [arXiv:hep-ph/9807278](#), [doi:10.1016/S0370-1573\(98\)00128-8](#). III A
- [85] N. Bartolo, V. De Luca, G. Franciolini, M. Peloso, D. Racco, and A. Riotto. Testing primordial black holes as dark matter with LISA. *Phys. Rev. D*, 99(10):103521, 2019. [arXiv:1810.12224](#), [doi:10.1103/PhysRevD.99.103521](#). III A, III A
- [86] Rong-Gen Cai, Shi Pi, Shao-Jiang Wang, and Xing-Yu Yang. Resonant multiple peaks in the induced gravitational waves. *JCAP*, 05:013, 2019. [arXiv:1901.10152](#), [doi:10.1088/1475-7516/2019/05/013](#). III A, III A, V
- [87] Michele Maggiore. Gravitational wave experiments and early universe cosmology. *Phys. Rept.*, 331:283–367, 2000. [arXiv:gr-qc/9909001](#), [doi:10.1016/S0370-1573\(99\)00102-7](#). III A
- [88] Latham A. Boyle and Paul J. Steinhardt. Probing the early universe with inflationary gravitational waves. *Phys. Rev. D*, 77:063504, 2008. [arXiv:astro-ph/0512014](#), [doi:10.1103/PhysRevD.77.063504](#). III A, III B
- [89] Shi Pi and Misao Sasaki. Gravitational Waves Induced by Scalar Perturbations with a Lognormal Peak. *JCAP*, 09:037, 2020. [arXiv:2005.12306](#), [doi:10.1088/1475-7516/2020/09/037](#). III A
- [90] M. C. Guzzetti, N. Bartolo, M. Liguori, and S. Matarrese. Gravitational waves from inflation. *Riv. Nuovo Cim.*,

- 39(9):399–495, 2016. [arXiv:1605.01615](#), [doi:10.1393/ncr/i2016-10127-1](#). III B, III B
- [91] Daniel G. Figueroa and Francisco Torrenti. Gravitational wave production from preheating: parameter dependence. *JCAP*, 10:057, 2017. [arXiv:1707.04533](#), [doi:10.1088/1475-7516/2017/10/057](#). III B
- [92] Chiara Caprini and Daniel G. Figueroa. Cosmological Backgrounds of Gravitational Waves. *Class. Quant. Grav.*, 35(16):163001, 2018. [arXiv:1801.04268](#), [doi:10.1088/1361-6382/aac608](#).
- [93] Rong-Gen Cai, Shi Pi, and Misao Sasaki. Universal infrared scaling of gravitational wave background spectra. *Phys. Rev. D*, 102(8):083528, 2020. [arXiv:1909.13728](#), [doi:10.1103/PhysRevD.102.083528](#). III B
- [94] Wen Zhao and Yang Zhang. Relic gravitational waves and their detection. *Phys. Rev. D*, 74:043503, 2006. [arXiv:astro-ph/0604458](#), [doi:10.1103/PhysRevD.74.043503](#). III B
- [95] C. J. Moore, R. H. Cole, and C. P. L. Berry. Gravitational-wave sensitivity curves. *Class. Quant. Grav.*, 32(1):015014, 2015. [arXiv:1408.0740](#), [doi:10.1088/0264-9381/32/1/015014](#). IV
- [96] Pau Amaro-Seoane, Heather Audley, Stanislav Babak, John Baker, Enrico Barausse, Peter Bender, Emanuele Berti, Pierre Binétruy, Michael Born, Daniele Bortoluzzi, et al. Laser interferometer space antenna. *arXiv preprint arXiv:1702.00786*, 2017. IV
- [97] Seiji Kawamura, Takashi Nakamura, Masaki Ando, Naoki Seto, Kimio Tsubono, Kenji Numata, Ryuichi Takahashi, Shigeo Nagano, Takehiko Ishikawa, Mitsuru Musha, et al. The japanese space gravitational wave antenna decigo. *Classical and Quantum Gravity*, 23(8):S125, 2006. IV
- [98] Kent Yagi and Naoki Seto. Detector configuration of DECIGO/BBO and identification of cosmological neutron-star binaries. *Phys. Rev. D*, 83:044011, 2011. [Erratum: *Phys.Rev.D* 95, 109901 (2017)]. [arXiv:1101.3940](#), [doi:10.1103/PhysRevD.83.044011](#). IV
- [99] Vincent Corbin and Neil J. Cornish. Detecting the cosmic gravitational wave background with the big bang observer. *Class. Quant. Grav.*, 23:2435–2446, 2006. [arXiv:gr-qc/0512039](#), [doi:10.1088/0264-9381/23/7/014](#). IV
- [100] Gregory M Harry, Peter Fritschel, Daniel A Shaddock, William Folkner, and E Sterl Phinney. Laser interferometry for the big bang observer. *Classical and Quantum Gravity*, 23(15):4887, 2006. IV
- [101] Benjamin P. Abbott et al. Upper Limits on the Stochastic Gravitational-Wave Background from Advanced LIGO’s First Observing Run. *Phys. Rev. Lett.*, 118(12):121101, 2017. [Erratum: *Phys.Rev.Lett.* 119, 029901 (2017)]. [arXiv:1612.02029](#), [doi:10.1103/PhysRevLett.118.121101](#). IV
- [102] B. P. Abbott et al. Prospects for observing and localizing gravitational-wave transients with Advanced LIGO, Advanced Virgo and KAGRA. *Living Rev. Rel.*, 21(1):3, 2018. [arXiv:1304.0670](#), [doi:10.1007/s41114-020-00026-9](#). IV
- [103] M Punturo, M Abernathy, F Acernese, B Allen, Nils Andersson, K Arun, F Barone, B Barr, M Barsuglia, M Beker, et al. The einstein telescope: a third-generation gravitational wave observatory. *Classical and Quantum Gravity*, 27(19):194002, 2010. IV
- [104] B. Sathyaprakash et al. Scientific Objectives of Einstein Telescope. *Class. Quant. Grav.*, 29:124013, 2012. [Erratum: *Class.Quant.Grav.* 30, 079501 (2013)]. [arXiv:1206.0331](#), [doi:10.1088/0264-9381/29/12/124013](#). IV
- [105] Benjamin P Abbott et al. Exploring the Sensitivity of Next Generation Gravitational Wave Detectors. *Class. Quant. Grav.*, 34(4):044001, 2017. [arXiv:1607.08697](#), [doi:10.1088/1361-6382/aa51f4](#). IV
- [106] David Reitze et al. Cosmic Explorer: The U.S. Contribution to Gravitational-Wave Astronomy beyond LIGO. *Bull. Am. Astron. Soc.*, 51(7):035, 2019. [arXiv:1907.04833](#). IV
- [107] Zaven Arzoumanian et al. The NANOGrav 12.5 yr Data Set: Search for an Isotropic Stochastic Gravitational-wave Background. *Astrophys. J. Lett.*, 905(2):L34, 2020. [arXiv:2009.04496](#), [doi:10.3847/2041-8213/abd401](#). IV
- [108] V. De Luca, G. Franciolini, and A. Riotto. NANOGrav Data Hints at Primordial Black Holes as Dark Matter. *Phys. Rev. Lett.*, 126(4):041303, 2021. [arXiv:2009.08268](#), [doi:10.1103/PhysRevLett.126.041303](#). IV
- [109] Gemma Janssen et al. Gravitational wave astronomy with the SKA. *PoS, AASKA14:037*, 2015. [arXiv:1501.00127](#), [doi:10.22323/1.215.0037](#). IV
- [110] George Hobbs, A Archibald, Zaven Arzoumanian, D Backer, M Bailes, NDR Bhat, M Burgay, Sarah Burke-Spolaor, D Champion, I Cognard, et al. The international pulsar timing array project: using pulsars as a gravitational wave detector. *Classical and Quantum Gravity*, 27(8):084013, 2010. IV
- [111] Ya B Zel’dovich and Igor D Novikov. The hypothesis of cores retarded during expansion and the hot cosmological model. *Soviet Astronomy*, 10:602, 1967. V
- [112] Stephen Hawking. Gravitationally collapsed objects of very low mass. *Monthly Notices of the Royal Astronomical Society*, 152(1):75–78, 1971. V
- [113] B. J. Carr, Kazunori Kohri, Yuuiti Sendouda, and Jun’ichi Yokoyama. New cosmological constraints on primordial black holes. *Phys. Rev. D*, 81:104019, 2010. [arXiv:0912.5297](#), [doi:10.1103/PhysRevD.81.104019](#). V
- [114] Misao Sasaki, Teruaki Suyama, Takahiro Tanaka, and Shuichiro Yokoyama. Primordial black holes—perspectives in gravitational wave astronomy. *Class. Quant. Grav.*, 35(6):063001, 2018. [arXiv:1801.05235](#), [doi:10.1088/1361-6382/aaa7b4](#).
- [115] Bernard Carr, Kazunori Kohri, Yuuiti Sendouda, and Jun’ichi Yokoyama. Constraints on primordial black holes. *Rept. Prog. Phys.*, 84(11):116902, 2021. [arXiv:2002.12778](#), [doi:10.1088/1361-6633/ac1e31](#). V
- [116] Eric Thrane. Measuring the non-Gaussian stochastic gravitational-wave background: a method for realistic interferometer data. *Phys. Rev. D*, 87(4):043009, 2013. [arXiv:1301.0263](#), [doi:10.1103/PhysRevD.87.043009](#). V
- [117] Rong-gen Cai, Shi Pi, and Misao Sasaki. Gravitational Waves Induced by non-Gaussian Scalar Perturbations. *Phys. Rev. Lett.*, 122(20):201101, 2019. [arXiv:1810.11000](#), [doi:10.1103/PhysRevLett.122.201101](#).
- [118] Peter Adshead, Kaloian D. Lozanov, and Zachary J. Weiner. Non-Gaussianity and the induced gravitational wave background. *JCAP*, 10:080, 2021. [arXiv:2105.01659](#), [doi:10.1088/1475-7516/2021/10/080](#). V